

Optical nanostructures design, fabrication, and applications for solar/thermal energy conversion

Mool C. Gupta,^{1,*} Craig Ungaro,¹ Jonathan J. Foley IV,² and Stephen K. Gray^{3,†}

¹*Department of Electrical & Computer Engineering, University of Virginia, Charlottesville, Virginia, 22901, USA*

²*Department of Chemistry, William Paterson University, 300 Pompton Road, Wayne, NJ, 07470, USA*

³*Center for Nanoscale Materials, Argonne National Laboratory, 9700 South Cass Avenue, Argonne, IL, 60439, USA*

**mgupta@virginia.edu*

†gray@anl.gov

Abstract

Optical nanostructures can control the optical absorption and emission properties of surfaces and are therefore being investigated for solar thermophotovoltaics, thermophotovoltaics, solar thermal, infrared sensing, infrared sources, incandescent light sources, and thermal imaging applications, among many others. This review article describes various modeling methods available for design of optical nanostructures to control light absorption and emission properties of surfaces, as well as various methods available for the fabrication of large area nanostructured surfaces. Throughout the review, we provide examples of state of the art energy generation devices using such optical nanostructures. A discussion of outstanding obstacles for the achievement of high efficiency solar thermophotovoltaics systems is provided along with examples of systems showing exceptional promise.

Key words: Optical design and fabrication, Optical Devices, Optics at surfaces, Thin Films, Solar Energy, Subwavelength structures, nanostructures

1. Introduction

Recently, there has been strong research activity in solar thermal (ST) [1, 2], solar thermophotovoltaic (STPV) [3, 4, 5, 6], and thermophotovoltaic (TPV) [7, 8] systems for converting solar and heat energy to electricity. While hybrid PV and ST systems which convert some or all incident energy to heat for direct use (such as in a hot water heater) and in photovoltaic-thermal collectors have also seen significant advances, this review article focuses only on system which output electrical energy. Additionally, this article focuses on high temperature STPV and ST systems due to their potentially high efficiency. There is strong potential for growth in these areas, especially through the use of novel nanostructured surfaces to control light absorption and emission from surfaces and to achieve high efficiency. This spectral light control can be achieved by nanostructuring of surfaces, which can strongly modify their optical properties [9, 10, 11]. Recently, significant progress has been made in the modeling and fabrication of nanostructures to control optical absorption and emission properties of surfaces. Nanostructured surfaces, for example, can be designed to be significantly more absorbing than their flat counterparts. Similarly, surfaces can be designed to emit infrared radiation in a very narrow spectral range, providing spectrally selective surfaces [12, 13]. A schematic of an STPV device with a broad solar absorber in thermal contact with a selective emitter is shown in Figure 1A. Figure 1B and C show the change in emission spectra from a blackbody emitter to a selective emitter using optical nanostructures. Some typical nanostructures are depicted schematically in Fig. 2.

STPV, ST, and TPV systems all share common surfaces but operate under different conditions. ST and STPV systems offer an alternative to PV power generation in alternative energy systems. Since both are heat engines, they are bounded by the Carnot limit and can theoretically exhibit extremely high efficiencies under high (but attainable) operating conditions. Additionally, since both ST and STPV systems rely on elements heated to high temperatures via concentrated solar energy, they are easy to modify for thermal storage of en-

ergy [14, 15]. This would allow them to operate into the night. An advantage of ST systems over STPV systems is that ST systems do not require the use of PV cells. The PV cells in STPV systems are expensive and can limit overall system size. Conversely, an advantage of STPV systems over ST systems is that
35 STPV systems have no thermal fluid or moving parts. This leads to them being more stable and compact solutions. Overall, ST tends to lend itself to large, immobile power installations while STPV is better suited for small applications. TPV systems operate on the same principle as STPV systems, but rely on an external heat source instead of solar energy [16]. This allows them to be used
40 in energy reclamation systems.

While both ST and STPV systems are capable of efficiencies approaching 85%, only ST systems have yet been realized with high real-world efficiency [11, 17, 18]. This is due primarily to the challenges related to the extremely high temperature operation of STPV systems; it is the view of the
45 authors that this presents exciting opportunities for researchers in materials science, nanophotonics, and engineering to devise strategies for increasing the temperature stability of STPV components, and for increasing the performance of STPV components operating at lower temperature. STPV systems have many advantages, such as those listed in the previous paragraph, that make
50 them attractive for further development.

Control of light absorption and emission properties allows the design of high efficiency solar and thermal energy conversion devices. It also has applications in the development of high efficiency infrared sources, sensors, and incandescent light sources. Various approaches have been demonstrated for controlling
55 light absorption and emission from surfaces such as the use of photonic crystals [19, 20, 21, 22], optical metamaterials [23, 24, 25], nanoparticles [26, 27, 28, 29], multilayer thin films [30, 11] and micro/nano textured structures [31, 32, 33, 34]. This review article describes various modeling methods available for design of optical nanostructures to control light absorption and emission properties of sur-
60 faces, the various methods available for the fabrication of large area nanostructured surfaces, and provides some examples of high-efficiency, state of the art,

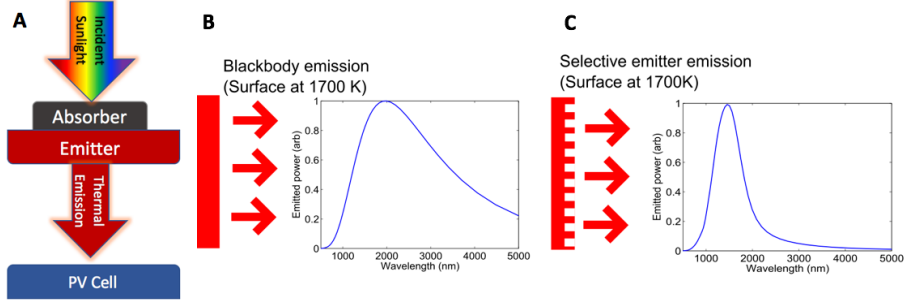


Figure 1: **A** Schematic of STPV system capable of reshaping the solar spectrum. **B** Spectral emission of a blackbody vs. **C** a selective emitter. Note that the scales on each graph are in different arbitrary units; the graph is intended to show the relative narrowness of the spectrum using the selective emitter.



Figure 2: Types of nanostructured absorbing and emitting surfaces: a) random nanotexture b) periodic nanotexture and c) dielectric/metal stack.

energy generation devices using such optical nanostructures. A path forward to more efficient solar and thermal energy generation devices using practical design methods and fabrication techniques is examined.

65 The limiting efficiency for ST and STPV systems with ideal absorbing and emitting surfaces comes from the Carnot efficiency (η) given by $\eta = 1 - \frac{T_c}{T_h}$, where T_c and T_h are the hot and cold temperatures, respectively. The absorbing surface efficiency is lowered due to radiative loss, given by $A\epsilon\sigma T^4$, where A is the area, ϵ is emissivity, σ is the Stefan-Boltzmann constant, and T is temperature. While
70 the Carnot efficiency of the system will increase with temperature, the absorbing surface efficiency will decrease due to increased emission from the absorbing surface at high operating temperatures [35]. The maximum operating efficiency of 85.4% is therefore reached at an operating temperature of 2600 K in the ideal case for both systems. Increasing the temperature beyond this will result in a
75 decrease in system efficiency. This analysis assumes that incoming radiation is concentrated to the maximum achievable solar concentration of 46000x. At this

concentration, the ideal surface is simply a blackbody absorber.

As the solar concentration is decreased, the ideal surface will be a blackbody absorber for wavelengths below some λ_{cutoff} , and an ideal reflector (generating
80 lower emission) for wavelengths above the cutoff. The location of λ_{cutoff} depends on the temperature of the system, the power density of the emission from the emitter, and the solar concentration levels achieved in the system. Typical λ_{cutoff} values will be close to $2\ \mu m$ due to the importance of absorbing a large portion of the solar spectrum [11].

85 In the case of STPV systems, the emitting surface will also play a role in device efficiency. The ideal surface will be a monochromatic emitter that emits radiation with energy equal to the bandgap energy of the PV cell used in the system [36, 35]. Unfortunately, monochromatic emitters have a power density of 0, resulting in the requirement of an infinitely large emitting surface for practical
90 power generation. Therefore, in practical STPV systems, an emitting surface with a small bandwidth will be desirable [11]. There also will be a certain system operating temperature that will lead to maximum operating efficiency due to competing effects between Carnot efficiency and heat loss due to thermal emission from the top surface [37, 38]. While it is true that the maximum
95 thermal emission per unit area of the STPV emitter will be lower than that of the sun (because it is bounded by blackbody emission at a temperature that is lower than the sun's temperature), the area of the emitter will be much higher than the absorber in a high-efficiency STPV system. Additionally, because the output spectrum of the STPV system is well-matched to the PV cell, and
100 thermalization losses are greatly reduced, there will be much less thermal energy absorbed by the PV cell. This results in a lower PV cell operating temperature and a reduced requirement for cell cooling. Figure 3 shows the evolution of maximum STPV system efficiency vs. temperature for an ideal system.

The temperature of $1000^\circ C$ was an upper limit chosen for practical ST systems based off existing technologies [17, 2]. This temperature was chosen for
105 the purpose of comparing different nanostructured surfaces suitable for incorporation into ST systems. The performance of ST systems will generally increase

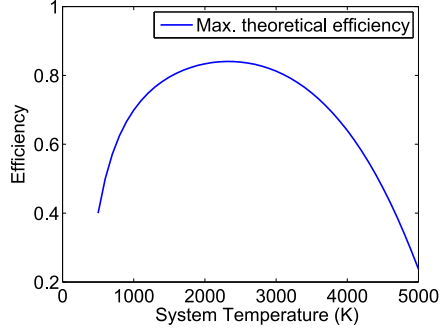


Figure 3: Maximum theoretical efficiency for various STPV system temperatures. This ideal limiting efficiency can be computed from the product of a Carnot efficiency for the system with an absorber efficiency which accounts for the radiative losses that the system will experience as a function of temperature. The fast increase around typical operation temperatures of STPV systems (1000-2000 K) reflects the Carnot contribution, and the decline starting at around 3000 K reflects the dominance of radiative losses at high temperatures. See Ref. [39] Chapter 4.1 for a detailed discussion of these limiting behaviors.

up to a specific temperature [40]. The value of this temperature is dependent on the quality of surfaces used and the solar concentration value achieved. For
110 tower-based (high-concentration) ST systems, this temperature is usually significantly above current operating temperatures, resulting in a desire for increased thermal stability. Most materials degrade at high temperatures for extended period of operation, so a reasonable number of 1000° was assumed. This number is consistent with temperature used in many solar thermal applications as
115 well as for thermophotovoltaics.

Figure 2 shows different kinds of nanostructures used to create spectrally selective surfaces in energy generation systems. Random and periodic nanostructures may have different shapes depending on the fabrication method used. Triangular, sawtooth, square, spherical, and cylindrical structures all see use in
120 these systems [41, 42, 11]. Additionally, spherical or obloid nanostructures may be embedded in a dielectric matrix to selectively scatter specific wavelengths of light. Lastly, as shown in Figure 2c, planar dielectric or dielectric and metal stacks may be used.

Melting point depression and thermal mismatching between layers makes
125 temperature stability a major concern for spectrally selective surfaces. This
issue is solved primarily through material selection and the use of protective
coatings on nanostructured materials [43]. Smaller nanostructures and thin-
ner layers can increase this effect, resulting in a limited design space for some
nanomaterials. Tungsten is a commonly used material for high temperature
130 systems due to its intrinsic thermal stability [44, 45]. However, care is required
when using tungsten at high temperatures as it is known to oxidize readily, and
several tungsten oxides are known to melt, or even evaporate, at low tempera-
tures [46]. There are several practical strategies which are effective in mitigating
this effect. One approach is to introduce an inert gas is done in the light bulb
135 industry, where only a partial vacuum is required to eliminate oxygen and water
and argon gas is used as the fill gas [47]. STPV systems need to be operated in a
partial vacuum to reduce convective losses regardless, so this particular strategy
does not represent an additional cost for these systems. Additionally, dielectric
coatings on tungsten may be used to protect tungsten from oxidation [43]; in
140 fact, the use of such coatings may be used to improves the emissive properties of
tungsten as was the case for several high-efficiency emitter structures reported
in table 2 [43, 48].

The type of nanostructure used in a system can have a large impact on its
ease of fabrication, spectral selectivity, and temperature stability. The use of
145 random elements in nanostructures eases fabrication tolerance requirements and
can improve selectivity, but can be difficult to design for or simulate properly
[49]. The presence of some smaller-period nanostructures can lead to lower
thermal stability in random nanostructures as well.

Square and cylindrical type gratings result in a rapid change in index of
150 refraction (as compared to tapered structures) that can result in low visible or
near infrared (IR) emittance and narrow absorption peaks [50, 51]. This can be
a boon to the design of narrow-band emitter structures, or a hindrance to the
design of solar absorbing surfaces. Combinations of multiple periods of gratings
can be used to broaden the emittance peaks in these structures; however, they

155 still lack high emission in the near IR and visible regions [52]. Using conical, sawtooth, or triangular type nanostructures can increase short-wavelength emission due to the more gradual change in index throughout the structure [53, 54]. Planar surfaces using thin layers of multiple different dielectrics suffer from relatively broad absorption peaks. The inclusion of a metallic layer or the addition
160 of many dielectric layers can result in a much more narrow emission peak [11].

There are many examples in the literature of nanostructures being applied to make high efficiency systems. Wang *et al.* [23] have demonstrated a highly efficient selective metamaterial absorber for high-temperature solar thermal energy harvesting. Using nanostructured titanium gratings on a MgF_2 spacer
165 deposited on W thin films was demonstrated with UV-near IR absorption of 0.9 and mid-IR emittance of 0.2. A structure with solar to heat conversion efficiency of 80% at 400°C was modeled and fabricated to achieve high solar light absorption efficiency over broad spectral wavelength range and emission surfaces emitting in a narrow band of wavelengths.

170 Spectrally selective surfaces have also been achieved by depositing nanoparticles on a surface and modifying surface morphology. Shah *et al.* [29] investigated spectrally selective surfaces for concentrated solar power receivers by laser sintering of tungsten micro and nanoparticles on a stainless steel substrate, resulting in a solar absorptance of 83% and thermal emittance of 11.6% at room
175 temperature. Multi-layer thin films of metal-dielectric coatings have also been shown to provide high broad wavelength solar absorption and low thermal emittance [30].

The use of theory and modeling has been critical to the design of these types of record-breaking structures, and will no doubt be critical moving forward as
180 the community continues to push the limits of conversion efficiency, durability, affordability, etc. In the following section, we will try to illustrate how theoretical electrodynamics techniques can be brought to bear to design these types of structures, as well as what challenges exist.

2. Design methodologies

185 2.1. Overview of the theoretical foundations of the optical properties of nanos- structures

Understanding how a nanostructured surface or particle absorbs, scatters, and/or reflects incident light provides critical information enabling the design of systems for efficient solar energy conversion. Calculating these quantities de-
190 pends upon the ability to solve Maxwell’s equations when light is incident upon nanostructures [55]. A wide variety of theoretical methodologies exist for solving Maxwell’s equations either in the time-domain (see for example [56, 57]), or in the frequency domain (see for example [58, 59, 60, 61, 62, 63]). Time-dependent approaches of solving Maxwell’s equations typically start from the first-order
195 time-dependent electric and magnetic field equations, whereas frequency domain methods usually take the second-order frequency-dependent wave equation, supplemented by appropriate boundary conditions, as their starting point.

In a few cases, Maxwell’s equations can be solved analytically; indeed, under some often reasonable approximations, the analytical solutions can even be writ-
200 ten simply, which greatly aids intuition about the behavior of a nanostructure. Two important analytical examples we will consider include the interaction of light with spherical nanostructures, solvable by Mie theory, and the interaction of light with planar nanostructures, solvable by the Transfer Matrix method. For more general structures, numerical techniques must be employed, and sev-
205 eral approaches have been put to considerable use. Here we will discuss the finite-difference time-domain (FDTD) method and the discrete dipole approximation (DDA); the former solves Maxwell’s equations in the time-domain, while the latter solves them in the frequency-domain. The finite element method, or FEM, is a frequency-domain approach capable of describing a greater variety
210 of problems [61]. The vectorial nature of Maxwell’s equations make implementations of FEM significantly more sophisticated than DDA. Rigorous coupled-wave analysis (RCWA) represents another frequency-domain method for solving Maxwell’s equations that is particularly relevant for periodic structures [62, 63]

and, because of its efficiency, has been used successfully to design absorber and
215 emitter structures for TPV/STPV applications, see for example [64, 65]. We
will also give several examples of applications of nanostructures for solar energy
conversion, focusing on which of the above methodologies are most appropriate,
and how they would be utilized for designing these nanostructures.

2.2. *Mie theory for spherical nanostructures*

220 Mie theory provides an analytical solution for Maxwell's equations when
light is incident upon a spherical particle. Analytical solutions are available for
not only homogeneous spheres but spheres composed of a core sphere with one
or more outer shells, and arbitrary complex dielectric constants may be used
to define the spherical systems. Quantities like the absorption, scattering, and
225 extinction cross section of the particle can be easily computed with Mie theory.
An excellent discussion of Mie theory, as well as practical source code, can be
found in [58].

While only rigorous for isolated spherical particles in homogeneous media,
judicious use of Mie theory can be an invaluable tool for modeling more com-
230 plicated structures. For instance, Mie theory can be adapted for very small
particles that can be modeled as ellipsoids, which includes nanodisks, nanorods,
etc. [58] Similarly, Mie theory can be combined with effective medium theories,
e.g. Maxwell-Garnett theory, to model regular or random arrays of particles on
a substrate, provided that the coupling between the neighboring particles is neg-
235 ligible [58]. Extensions to effective medium theories have also been developed
that account for the impact on near-neighbor coupling on the polarizability of a
spherical structure, including renormalized polarizability approaches of Mochán
and co-workers[66, 67], and dressed polarizability approaches of Yoo *et al.*[68].
These approaches offer similar simplicity of using Mie theory in conjunction
240 with an effective medium theory, but offer a more rigorous treatment of the
coupled optical response of the spherical particle to its neighbors.

2.3. Design of nanostructures for enhancing solar energy conversion using Mie theory

The relative simplicity of the theoretical framework describing scattering and absorption of spherical nanostructures affords the ability to design systems utilizing spherical nanoparticles for a variety of solar conversion applications. The scattering properties of spherical nanoparticles can be leveraged to concentrate and trap incident light into thin-film photovoltaic (PV) materials to increase their conversion efficiency. This strategy is particularly effective if the light scattering can occur only in the forward direction, increasing the flux of optical energy into an active PV material, for example [69]. Mie theory leads to the prediction of this particularly extreme form of anisotropy where the particles scatter light only in the forward direction when the coefficients for the electric and magnetic dipolar terms are identical, which is often called the first Kerker condition [70]. Physically, this can be understood as an interference between electric and magnetic dipolar resonances. Because this is a resonant effect, a given particle geometry will support such scattering behavior only at certain frequencies. Nevertheless, Mie theory computes these coefficients directly, and it is straightforward to develop a design protocol for spherical particles embedded in a medium with known optical properties (e.g. corresponding to the PV material, or a compatible substrate) that support these resonances at a desired frequency. The exceptionally large extinction cross sections of metal nanoparticles, due to their ability to support surface plasmons, can also be exploited to efficiently trap light across the solar spectrum. For example, the optical response of spherical dielectric-core metal-shell nanoparticles is highly tunable, and can be computed exactly with a generalization of Mie theory. Halas and co-workers have employed Mie theory to design optimal distributions of core-shell nanoparticles to enhance absorption over the AM 1.5 solar spectrum [71], where AM 1.5 indicates the standard for the solar spectrum after attenuation by Earth's atmosphere. Using a distribution of simple silica core/gold shell particles with modest coverage allowed absorption of 84% of incident solar power across the AM 1.5 spectrum [71]. Figure 4 shows the extinction efficiency computed by

Mie theory for various core-shell particle structures. Similarly, resonant or near-
 resonant scattering effects of spherical or cylindrical nanostructures, including
 275 nanowires, have been modeled within the framework of Mie theory to create
 exceptionally strong broad-band absorbing structures [72] and broad-band anti-
 reflection coatings [73], both of which are widely applicable to solar conversion
 technologies. Again, we emphasize that Mie theory is rigorous only in the limit
 of isolated particles, and cannot easily account for particle/interface effects.
 280 For such effects, more general numerical modeling approaches such as FDTD or
 DDA are required, and we discuss these approaches in Sections 2.6-2.8.

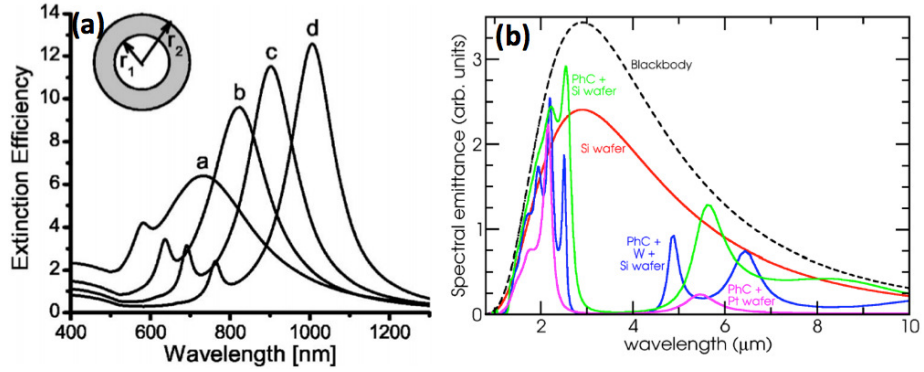


Figure 4: Illustration of radiation control using engineered spherical core-shell nanoparticles (a) and multi-layer planar film structures (b). The absorption, scattering, and extinction cross sections of the core-shell particles can be tuned across the solar spectrum by changing the ratio of the shell thickness (r_2) to the core radius (r_1), and these quantities can be computed using Mie theory (see Section 2.2) for isolated particles, or the DDA method (see Section 2.8) for assemblies of particles. In (a), the radius of a silica core is fixed at 60 nm, and the thickness of a gold shell is taken to be 80 nm for curve a, 70 nm for curve b, 67 nm for curve c, and 65 nm for curve d. The emittance of several multi-layer structures plotted in (b) can be simply computed using the Transfer Matrix Method (see Section 2.4); however, more sophisticated global device efficiency considerations were used to identify a photonic crystal on a platinum substrate (violet curve in (b) as the optimal emitter structure for an integrated STPV system [4]. Figures reproduced from [71] and [4] with permission.

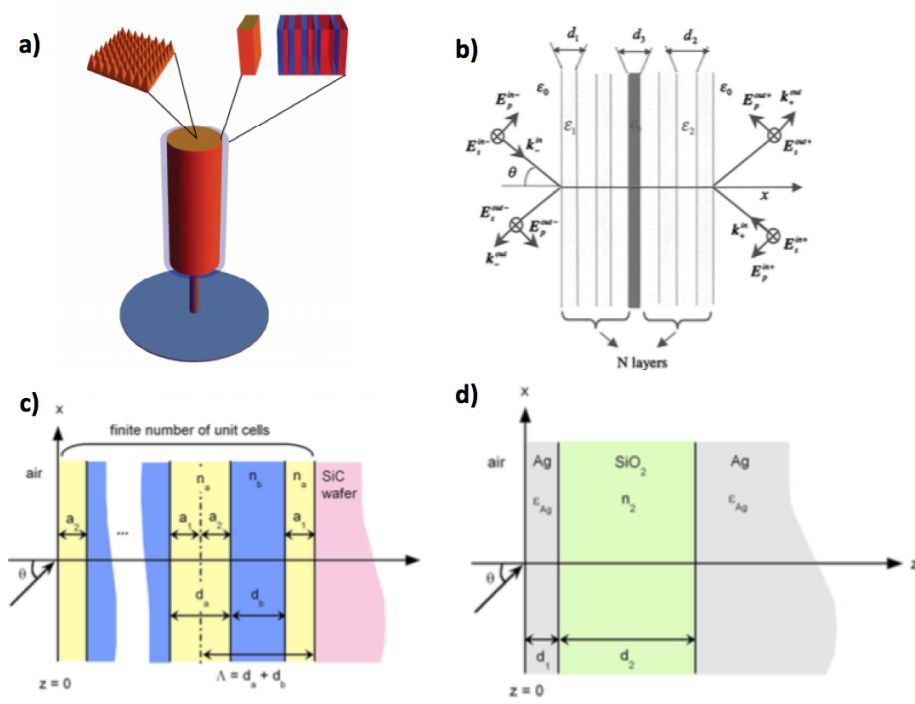


Figure 5: Illustration of various planar structures amenable to design and modeling by transfer matrix methods that serve as selective emitter structures. A 1D photonic crystal integrated into a STPV absorber/emitter structure is illustrated in (a). Further details, including absorptivity spectra from this class of structures, can be found in Fig. 6 and in [74]. A Bragg reflector with a single absorbing defect layer, which supports spectrally selective emission modes, is illustrated in (b). Further details, including emissivity spectra from this class of structures, can be found in [75]. A structure that achieves angular and spectral selectivity by coupling evanescent photonic crystal modes to surface phonon polariton modes in a polar layer is illustrated in (c). A structure that achieves angular and spectral selectivity by coupling incident light into Fabry-Pérot resonances is illustrated in (d). Further details, including emissivity spectra from these classes of structures, can be found in [76]. Figures reproduced from [74, 75, 76] with permission.

2.4. Transfer Matrix Methods for planar structures

For multi-layer planar structures, the fields can be written piece-wise as plane waves, and closed-form expressions for the wavevectors and amplitudes of the fields in each layer can be determined from considerations of Maxwell's

equations and appropriate boundary conditions. The boundary conditions can be expressed conveniently as matrix equations, and the amplitudes can be computed by straightforward matrix multiplication, which forms the basis of what is called the Transfer Matrix Method [59]. The general Transfer Matrix equations for an L -layer system can be written as

$$\begin{pmatrix} E_1^+ \\ E_1^- \end{pmatrix} = \begin{pmatrix} M_{1,1} & M_{1,2} \\ M_{2,1} & M_{2,2} \end{pmatrix} \begin{pmatrix} E_L^+ \\ E_L^- \end{pmatrix}, \quad (1)$$

where the elements $M_{i,j}$ depend on the material properties (the complex refractive index, $(\tilde{n} = n + ik)$ and geometry of each layer, as well as the frequency and polarization of incident light. The precise form of these elements can be found in the excellent treatment by Yeh [59], and this method has been successfully applied for designing multi-layer absorbing structures that find wide use in TPV/STPV applications [75, 76, 77]. We interpret E_1^+ and E_1^- as incoming and outgoing wave amplitudes on the incident side, respectively; similarly, E_L^- and E_L^+ are incoming and outgoing wave amplitudes, respectively, on the terminal side of the structure. With the access to the field amplitudes and wavevectors, a number of useful quantities may be computed. For example, the Fresnel reflection and transmission amplitudes may be computed as $r = E_1^-/E_1^+ = M_{2,1}/M_{1,1}$ and $t = E_L^+/E_1^+ = 1/M_{1,1}$, respectively. The reflection can then be calculated as $R = |r|^2$, the transmission as $T = |t|^2 n_L \cos(\theta_L)/(n_1 \cos(\theta_1))$, where n_i and θ_i denote the (real) refractive index of the material of layer i and the incident/refraction angle in layer i , respectively. For computing the Fresnel equations, the field amplitude E_L^- is set to zero. The absorption can simply be computed as $A = 1 - T - R$. An additional requisite assumption is that the semi-infinite bounding media (layer 1 and layer L) have real refractive indices. When this is the case, θ_L will be a real angle to satisfy conditions required by Snell's law for absorbing media [78, 79] until the transmitted wave becomes evanescent, as is the case for total internal reflection (when $\text{Re}(\theta_L) = 90^\circ$). In this case, the transmission is necessarily zero, so the interpretation of the transmission (T), which must be a real num-

ber between 0 and 1, is preserved in the Transfer Matrix Method for absorbing
 intermediate materials bounded by semi-infinite dielectric layers. That is, the
 Transfer Matrix Method allows all intermediate layers with finite thickness to
 have complex refractive indices and the fields to have complex angles of reflec-
 310 tion/transmission in the intermediate layers. Thus, the Transfer Matrix Method
 has been successfully applied for designing multi-layer absorbing structures that
 find wide use in TPV/STPV applications [75, 76, 77]. The computational effort
 of the Transfer Matrix Method is minimal as it primarily involves the compu-
 tation of the matrix elements $M_{i,j}$, which can be accomplished in a number
 315 of arithmetic operations that scales linearly with the number of layers in the
 structure. The Transfer Matrix Equations can also be used to compute the
 dispersion for resonant modes in multi-layer structures. Two resonant modes of
 particular interest for multi-layer structures with one or more absorbing layers
 include surface plasmon polariton (SPP) modes [80, 81, 82, 69, 83], and per-
 320 fectly absorbing (PA) modes [84, 85, 86, 83]. SPP modes occur when $R \rightarrow \infty$
 and $T = 0$, while the latter occurs when $R \rightarrow 0$ and $T = 0$ [83]. SPPs in-
 volve collective electronic oscillations coupled to a propagating electromagnetic
 wave, and they allow light to be guided along the 2-dimensional interface be-
 tween a metal and a dielectric layer. Because SPP wavevectors lie beyond the
 325 light-line (i.e. they have wavevector magnitudes larger than that of light prop-
 agating in the dielectric layer), excitation of SPPs can occur only under certain
 conditions. A classic technique for exciting SPPs, known as the Kretschmann-
 Raether configuration [87], involves an asymmetric dielectric/metal/dielectric
 structure with the refractive index of the dielectric substrate being larger than
 330 the refractive index of the dielectric superstrate. While normally incident light
 cannot couple into SPPs on specular surfaces, it can couple into SPP modes at
 the metal/superstrate interface if it is incident from substrate side at an appro-
 priate angle. Using the Transfer Matrix Method to find the complex wavevector
 components that lead to the SPP condition ($R \rightarrow \infty$ and $T = 0$) in such an
 335 asymmetric structure is equivalent to finding the angle that allows coupling
 of light into the SPP via Kretschmann-Raether excitation. [87, 83] Scattering

at the surfaces, for example because of surface roughness or patterning with nanoparticles, can also produce large wavevector components that will allow light to couple into SPPs even at normal incidence. Perfectly absorbing modes
340 can allow perfect absorption of incident light by thin absorbing layers. Unlike SPPs, PA modes are non-propagating and do not necessarily lie to the right of the light line; in these cases, light can couple into perfectly absorbing modes in symmetric structures. [83]

2.5. *Design of selective emitters for thermophotovoltaic applications using Transfer Matrix Methods*

345

The resonant properties of multi-layer planar structures can be exploited for designing highly-selective emitter structures for use in thermophotovoltaic (TPV) and STPV devices. In TPV devices, thermal energy is transferred to a spectrally-selective emitter structure. The radiation wavelength of the emitter
350 should be well matched to a PV cell bandgap so that its thermal emission can be efficiently converted to electrical current. TPV systems can harvest thermal energy as waste heat from engines or other sources. An STPV system is simply a TPV system that harvests thermal energy from solar radiation, and involves a good solar absorber as one of its components. The design of both absorber
355 and emitter structures has been the focus of considerable theory and modeling effort. Figure 5 illustrates several optimized planar emitters that were designed using Transfer Matrix Methods [75, 76, 11].

Despite their simplicity, multi-layer planar structures can support a rich number of interesting and controllable optical phenomena which can be ex-
360 ploited for TPV and STPV applications. One-dimensional photonic crystals (1DPCs) can be used in conjunction with absorbing materials to enhance the spectral and/or angular selectivity of absorption and emission [74] in an integrated absorber/emitter STPV structure. The evanescent modes supported by 1DPCs can also enable coupling into resonant surface waves in near and
365 mid-IR frequencies, including surface plasmon polariton and surface phonon polariton modes, respectively [76], which gives hybrid structures consisting of

hybrid 1DPCs and either a metal (strong near IR absorber) or a polar material (strong mid IR absorber) exceptional angular and spectral selectivity. Similarly, Ben-Abdallah and Ni have shown that coupling between localized defect states and surface waves can give rise to strong spectrally coherent emission when a single absorbing defect layer is introduced into a Bragg stack [75]. The RCWA method has also been applied with success to both 1D and 2D periodic structures for selective absorber and emitter structures [64, 65]. More details about the theory and implementation about this method can be found in [62, 63].

Given the diversity of possible planar structures, a vast parameter space exists for their design, and optimization methodologies must be chosen judiciously. Drevillon and Ben-Abdallah [88], as well as Nafzaoui, Drevillon, and Joulain [89], have developed robust optimization methodologies that steer multi-layer structures to an optimal emissivity profile. The optimum of the emissivity profile can be defined in a variety of ways with respect to variables including the PV cell and operating conditions. One such approach for defining such a profile involves using the ultimate efficiency of the emitter as a figure-of-merit, where the ultimate efficiency depends on the emissivity of the structure, the band-gap of the PV cell, and the target temperature of operation (see section 4.2). The emissivity can be computed from the reflectance and transmission using the Transfer Matrix Method, enabling efficient computation of the figure-of-merit. The design problem can then be formulated as a maximization of the figure-of-merit in terms of the geometry and material properties of the emitter structure. This approach has been employed to design 1D photonic crystals involving tungsten and dielectric layers with ultimate efficiencies of about 53% [90] (see Table 2). Similarly, the Transfer Matrix Method can be used to design broad-band absorbers, and has led to the prediction of absorption efficiencies of 74% in 1D photonic crystals made of tungsten and dielectric layers [90] (see Table 1).

A different Transfer Matrix Method-based approach for the design of STPV components, recently introduced by us, leverages the observation that structures that support perfectly absorbing modes with certain characteristics can

perform as exceptional selective emitters. These characteristics, described in detail in [77], can be encoded directly into a search routine that allows for the
400 identification of structure geometries that support these modes. The optimization over the figure-of-merit is therefore replaced with a search for a zero in T and R , which is equivalent to finding a zero in the transfer matrix element $M_{2,1}$ under the condition that the transmission is also zero, which can be easily satisfied. This approach has predicted structures with ultimate efficiencies
405 of 68% at operating temperatures of 1750 K when coupled with common PV materials [77]. The TMM has also been applied by Karalis and Joannopoulos to the design of planar emitter/PV cell systems separated by subwavelength gaps that exploit near-field radiative heat transfer effects, which can exceed the far-field limit bounded by the Planck blackbody law [91]. In their approach,
410 the dispersions of the planar emitter and PV cell are designed such that radiative coupling between the two is only allowed at a frequency just above the PV bandgap [91].

2.6. Finite-Difference Time-Domain method

For the optical behavior of more general structures, numerical approaches
415 must be employed to solve Maxwell’s equations. Perhaps the most conceptually simple approach is known as the finite-difference time-domain (FDTD) method. Here the time evolution of the fields is computed using Maxwell’s equations (the curl equations) where the spatial and temporal variables are discretized on a rectangular grid, and centered finite-differences are used for the derivatives in
420 terms of these variables [56]. The electric and magnetic fields are spatially staggered on the computational grid, which enforces Gauss’ law. Quantities such as absorption, scattering, reflection, and transmission can be defined in terms of fluxes of electromagnetic fields. Electric field distributions and other quantities may be obtained in the frequency domain by the appropriate Fourier transform
425 of the time-domain fields. The permittivity of metals and semiconductors can have strong frequency dependence across the UV/Vis/IR spectrum, and this frequency dependence requires some consideration for time-domain simulations

like FDTD. Material dispersion leads to time-dependence of the material susceptibility and causes the polarization density to depend on field values at all
430 previous times. This is commonly handled by fitting the permittivity to an analytical function of frequency, commonly a sum of Drude and Lorentz oscillator functions, so that the convolution can be easily computed. A practical drawback is that it can be difficult to obtain a good fit for these functions across a broad spectrum for highly-dispersive materials.

435 The computational effort of FDTD scales with the 4^{th} power of the computational domain for simulations with 3 spatial and 1 temporal dimension. The spatial grids are generally discretized with grid spacing d , where d is a value less than the sub-wavelength electromagnetic field variations of interest in the complex optical response media being studied. (In such media, suitable values of d such that the results are converged must be determined empirically.)
440 The time-step is usually defined relative to the spatial grid size by the Courant factor [56]. This tends to make simulations of structures with several disparate length-scales challenging, as a small grid size is required for the smallest feature, while many grid elements are required to span the physical structure. However,
445 FDTD implementations can utilize multi-resolution grids to reduce the computational effort in these cases. Furthermore, FDTD simulations can exploit symmetry, periodicity, and can be massively parallelized, all of which has enabled their application to a variety of complex systems. Of particular relevance to modeling the emission from the nanostructures of interest are recent FDTD
450 developments that allow direct FDTD modeling of emissivity and near-field radiative heat transfer[92, 93, 94, 95]. These recent developments, termed fluctuational electrodynamics, have enabled systematic modeling of systems where the emitter structures are separated from the PV cell by sub-wavelength gaps, and have guided the design of experimental systems showing significant enhancement in heat transfer compared to systems that rely on far-field radiative
455 transfer [96].

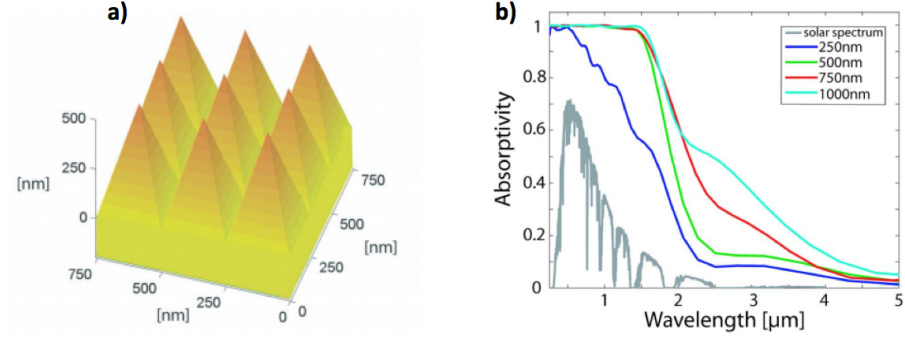


Figure 6: Illustration of a tungsten structure whose absorptivity can be tuned by patterning of the surface. In this example, the tungsten structure is patterned with nanopyramids with various pyramid heights and with period fixed at 250 nm. A representative structure with a pyramid height of 500 nm is shown in (a). Absorptivities of textured tungsten structures are plotted in (b) for a variety of pyramid heights with the period of the pyramids fixed at 250 nm. The finite-difference time-domain (FDTD) method was used to compute the absorptivities shown in (b). Figures reproduced from [11] with permission.

2.7. Design of patterned structures for absorption enhancement using the FDTD method

Extensions of the previously-discussed multi-layer planar structures involve
 460 introducing geometric features in the lateral dimension(s). These types of structures include 2D and 3D photonic crystals, metasurfaces, metamaterials, and random-textured materials. FDTD can be a powerful tool for designing these types of structures, and can be particularly efficient when symmetry and/or periodicity can be exploited. Often, these sorts of patterned materials are desired
 465 to enhance the absorption of visible light, for example, to design a perfect absorber across the solar spectrum for solar thermophotovoltaic applications. For such an application, the transmission, reflection, and absorption can be computed across the spectrum as features of the surface are varied. This procedure is illustrated in Figure 6 (a) and (b), where the absorptivity of a tungsten surface
 470 patterned with pyramidal structures is computed by the FDTD method [74]. Similarly, Atwater and co-workers have employed FDTD simulation to design ultra-thin patterned surfaces that behave as broad-band “super absorbers” ca-

pable of enhancing conversion efficiency in thin-film PV materials [97]. Several of the current authors have utilized FDTD simulations to study and design tungsten absorber surfaces patterned with nanocones with absorption efficiencies of 80% [49] (see Table 1), as well as tungsten blazed grating emitter surfaces with ultimate efficiencies of 59% [54] (see Table 2).

Many codes like Lumerical [98], a commercial-grade FDTD simulator, and MEEP [57], an open-source FDTD code, have scripting capabilities and other built-in tools to perform sweeps and optimizations over system variables, including material constants and geometric parameters. These sorts of scripting interfaces also allow the computation of more sophisticated quantities; for example, the net energy flux between isolated structures may be desired to optimize near-field radiative heat transfer [93].

2.8. Discrete Dipole Approximation

Several computational methodologies for solving Maxwell's equations in the frequency domain are also available, and here we focus on the Discrete Dipole Approximation (DDA), which is particularly useful for problems involving scattering and light absorption from particles. The idea behind DDA is to represent scattering structures by an array of N dipoles. It is important to note that in practice N is generally large, i.e. the particle or particles in the problem are being described by many dipoles filling their volumes and so that multipolar interactions can be correctly described. DDA is thus routinely used as a rigorous computational electrodynamics method and so its name is somewhat deceptive.

In DDA, each dipole has a polarization given by $\mathbf{P}_j = \alpha_j \mathbf{E}_j$, where \mathbf{E}_j is the electric field at the discrete point occupied by dipole j , and α_j is the polarizability of dipole j , which is determined from the permittivity of the material being modeled [60]. The electric field at the position j of a given dipole is expanded as

$$\mathbf{E}_j = \mathbf{E}_{inc,j} - \sum_{k \neq j}^N \mathbf{A}_{j,k} \mathbf{P}_k. \quad (2)$$

The incident field ($\mathbf{E}_{inc,j}$) has the form of a monochromatic plane wave, and

the product $-\mathbf{A}_{j,k} \mathbf{P}_k$ gives the electric field at point j due to the polarization at point k ; hence, the matrix \mathbf{A} carries information about the geometry and polarizability of the dipoles. The polarization is found by solving the system of linear equations given by $\sum_{k=1}^N \mathbf{A}_{j,k} \mathbf{P}_k = \mathbf{E}_{inc,j}$, where the diagonal elements of \mathbf{A} have the known form $\mathbf{A}_{jj} = \alpha_j^{-1}$. Iterative methods are used to solve this equation, leading to overall quadratic scaling of the computational effort with the number of dipoles [60]. The optical cross sections may be written in terms of the polarization of the dipoles [60].

In general, high resolution can be obtained for small structures with a relatively small number of dipoles, and so DDA can be extremely efficient for modeling the optical properties of nanoparticles. DDAs formulation in the frequency domain also makes it more convenient than FDTD for modeling materials whose permittivity depends strongly on frequency since the permittivity as a function of frequency can be fed directly into the simulation. While scattering is solved for one frequency at a time, DDA can be run in parallel over the desired frequency range. One considerable drawback is that convergence of the DDA method, both in terms of the number of iterations for solving the linear equations and in terms of the accuracy of the polarization with respect to the number of dipoles, can be quite challenging for materials with large real or imaginary components of refractive index [99]. Silver is a classic material for which DDA modeling presents a particular challenge at visible frequencies.

Interesting recent developments in DDA of relevance to the problems of concern in this review include variations of DDA that are capable of describing particle-surface interactions [100] and near-field radiative heat transfer [101].

2.9. Design of nanostructures for near-field enhancement of solar energy conversion using the DDA method

Concentration of incident optical energy into the near-field of localized surface plasmons supported by nanostructures can also be leveraged to enhance solar conversion efficiency in PV materials. This approach is complementary to the one discussed with anisotropic scattering because it exploits the absorption

of the nanostructure(s) rather than the scattering. The optical energy concentrated in the near-field of the plasmon can directly excite particle-hole pairs in a PV material with high efficiency if the absorption rate of the PV material is larger than the plasmon damping rate (equivalently, the inverse lifetime of the plasmon excitation) [69]. Therefore, nanoparticle systems with high near-field intensities and long plasmon lifetimes are ideal for these applications. The large cross sections of plasmonic particles can also be leveraged to increase absorption efficiency in absorber structures in STPV applications. DDA methods can efficiently compute near-field distributions, absorption cross sections, etc, for multiple particles with complex geometries and sharp asperities that are separated by small-gaps, which are structures that typically give rise to exceptional near-field enhancement and large absorption cross sections. Plasmon lifetime information can be obtained from a Fourier transform over the absorption spectrum that is generated directly by DDA simulations run over a desired frequency range. Because the DDA method captures the fully coupled optical response of assemblies of nanostructures, it could be used to obtain an exact description of the absorption efficiency of the distribution of core-shell nanoparticles leveraged by Halas and co-workers for absorption enhancement [71] (see Figure 4).

2.10. Summary and outlook for theoretical design methodologies

We have described a number of powerful theoretical methodologies that can be put to use to understand, predict, and even tailor the optical response of systems of simple or complex nanostructures. The use of these methods, along with the ingenuity of many researchers, has allowed the design of many novel and useful systems for radiative control. However, as will be discussed in more detail in the remaining sections, overall conversion efficiencies of TPV/STPV systems often fall around 3-8%, well short of the theoretical limit of 85%. A significant challenge remains in integrating various theoretical methodologies to model and optimize global device performance [4, 10]. In principle, nanostructured systems may be designed or discovered by coupling the various electrodynamics modeling approaches described above to global optimization methods. Generally,

an appropriate figure-of-merit to be maximized is identified, e.g. the ultimate efficiency which will be discussed in detail later, and repeated calculations of the figure-of-merit are carried out while adjusting the features of the nanostructure until a global optimum is found. A plethora of multi-parameter optimization

560 methods are available and have been used in the context of optimizing the optical response of nanostructures, including clustering algorithms [4], the Simplex method [102, 71], genetic algorithms [103, 88], particle swarms [89, 104], and Gaussian process modeling [105]. Certainly one challenge is that an integrated TPV/STPV system must couple together various optical modalities for absorption and emission. Usually, this requires abandoning exact analytical approaches

565 in favor of approximate (e.g. perturbative) analytical approaches like coupled-mode theory. Alternatively, researchers must rely on the use of the numerical methodologies described above, though this may prove daunting from a computational point of view due to the multi-scale nature of these systems. Global system optimization must also include considerations like thermal management

570 along with electrodynamics, as the requisite operating temperatures can lead to oxidation or deformation of the constituent structures and degradation of the device performance. Consideration of these various system parameters creates a highly heterogeneous optimization problem and presents significant challenges for global optimization. However, several authors including Celanovic and co-workers [4] as well as Wang and co-workers [10] have taken on the challenge of

575 designing systems with optimal device consideration, which have led to device efficiencies approaching 3% and 10%, respectively. Considering recent interest in exploiting near-field radiative heat-transfer to enhance TPV/STPV power and conversion efficiency [106, 96, 91], we anticipate that modeling methods that

580 utilize fluctuational electrodynamics [92, 93, 94, 95, 101] will become increasingly important. Similarly, appropriate modeling of radiative, electrical, and thermal loss mechanisms will be critical for helping to bridge the gap between theory and experiment in the field [107].

3. Large area fabrication of optical nanostructures

3.1. Direct laser writing and laser interference lithography

A high power laser beam focused to sub-micron dimensions allows direct ablation of surface material, as shown in Figure 7(a), to form periodic or non-periodic structures. Alternatively, selective exposure of a photoresist can create feature sizes of about 0.5 microns [108]. Though these fabrication techniques are limited to structure sizes on the order of 1 cm^2 , we note that in solar thermophotovoltaics the incident sun light is highly concentrated with concentration factor of many 1000 times, so the focused light beam size is relatively small (less than an inch in diameter). Therefore, STPV structures with relatively small absorber and emitter components can generate reasonable power output. In terms of reduction of cost, one can consider utilizing an imprinting process using a master for low cost fabrication process.

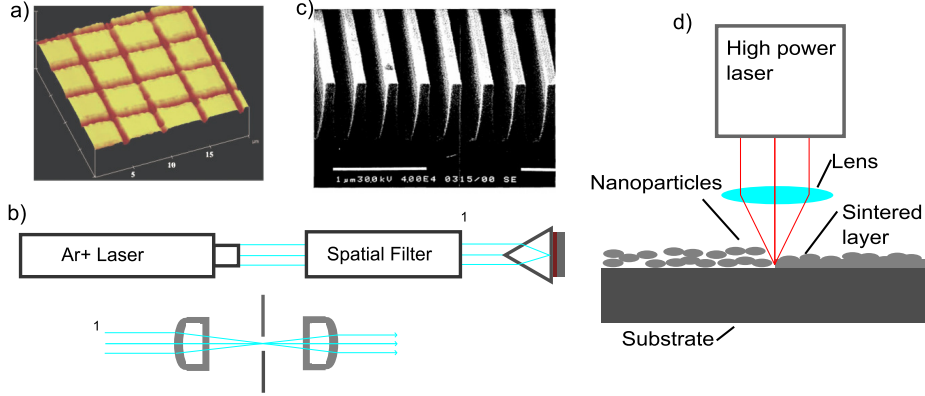


Figure 7: a) AFM photograph of a micromachined double periodic structure with line-widths less than a micron [108] (reproduced with permission), b) Experimental setup for laser interference lithography, c) SEM image of gratings fabricated by laser interference lithography and etched into quartz [109] (reproduced with permission), and d) experimental setup for laser sintering of nanoparticles.

To obtain feature sizes of few hundred nanometers over a large area, laser interference lithography is ideal [109]. In interference lithography, a laser beam is split into two components, which can be recombined to form an interference

pattern, as shown in Figure 7(b).

The period, P , of the grating is determined by $P = \frac{\lambda}{2n \sin(\theta)}$ where λ is the wavelength of the laser light, n is the refractive index of the medium and θ is the angle between two beams. For a wavelength of 442 nm, a surrounding medium index of 1.5, and an angle between the two beams of 60 degrees, line-widths of about 200 nm will be generated. Figure 7(c) shows a scanning electron microscope (SEM) image of the periodic pattern obtained with a He-Cd laser. This technique can allow the fabrication of large area patterns on various substrates. An exposed photoresist mask is used to etch the pattern on the substrate materials.

This method will be well suited for the fabrication of spectrally-selective surfaces as needed for STPV and TPV systems. The selective spectral emission wavelength and the efficiency of the emission can be controlled by the period, height and spacing between lines.

3.2. Laser sintering of nanoparticles

To achieve nanoscale roughness, nanoparticles dispersed in a liquid can be coated on a substrate [110]. A laser sintering process is then used to fuse the nanoparticles together by the high temperature generated by laser light absorption. In this process, the nanoparticles also get bonded to the substrate. The laser sintering process is shown in Figure 7(d). By controlling laser processing parameters such as optical power, scan speed, and beam overlap, different surface morphologies can be achieved. This fabrication method is well suited for solar thermal applications where high solar absorptance and low thermal emission is required.

3.3. Glancing angle deposition (GLAD)

Highly light-absorbing surfaces can be generated by micro-scale roughness due to the multiple reflections within such surfaces that effectively trap the incident light. Thin films of various materials, when deposited at large angles of incidence relative to the substrate and under vacuum conditions, give rise

630 to cone like structures as shown in Figure 8(a) [111]. The deposited films look black to the naked eye because of their extremely high optical absorption. The absorption efficiency of these structures can be controlled by the height of, and spacing between, the pillars. The glancing angle deposition method can be used to enhance solar light absorption and to fabricate spectrally-selective surfaces

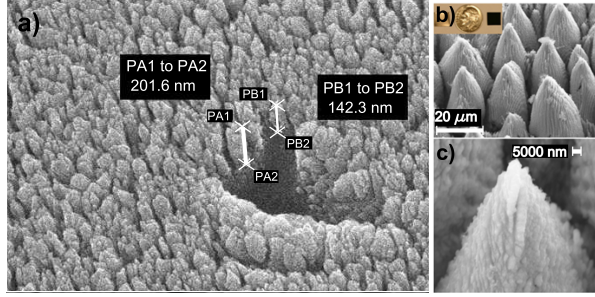


Figure 8: a) SEM image of GLAD structures (reprinted with permission) [112] and b) and c) SEM images of a laser micro/nano textured Ti surface (reprinted with permission) [34].

635 3.4. Laser micro/nano textures

Micro- and nano-textured surfaces can be obtained when a high power laser beam is focused on a substrate and laser processing is carried out within a certain power and scan speed range [34]. The details of the texture, including height and spacing, can be controlled by laser processing parameters. The properties of the textured surface allow control over the absorption efficiency of the surface. 640 Figure 8(b) and 8(c) show SEM images of a laser microtextured Ti surface.

Multi-layer thin films composed of metal dielectric layers can also be designed such that high optical absorption can be achieved. Reciprocally, the emissivity of multi-layer structures can be tuned over a narrow spectral range. Figure 2(c) 645 shows an example of thin film structure to control the emission properties.

The high solar radiation absorption can be achieved by fabrication techniques such as metal-dielectric multi-layer structures, surface microtexturing and by the use semiconductor-metal layer structures. The spectral selective emittance can be achieved by fabrication of photonic crystal structures using

650 standard optical or e-beam lithography method or by the use of periodic/non-periodic submicron surface textures. The microtexture fabrication method is suited to achieve black surfaces with extremely high ($>95\%$) light absorption over broad wavelength and incident angle ranges.

4. Solar energy conversion applications

655 4.1. Solar thermal

Solar thermal (ST) systems are solar powered devices that generate energy via a heat engine. Incoming solar energy is concentrated on an absorbing surface, which is heated to high temperatures. A heat exchange fluid is then used to draw energy from the absorbing surface to the heat engine. Since heat engines can be more efficient at higher operating temperatures, it is important for 660 ST systems to remain stable at high temperatures, up to 1000°C . While current TPV technology allows for high absorbance (>0.9), low thermal emission (<0.1), and thermal stability (in evacuated tubes) at low operating temperatures (about 400°C), overall system efficiency can be greatly improved by increasing temperatures [113, 114]. Unfortunately, current technologies lack thermal stability and 665 will have high thermal emission under these conditions [115].

Because they operate at high temperatures, absorbing surfaces will lose energy through thermal emission. To reduce this loss, the thermal emittance of the absorbing surface must be minimized. Here, we will define ϵ_{abs} as the thermal 670 emittance of an absorbing surface held at a specific temperature relative to the thermal emittance of a blackbody held at the same temperature. This means that an absorbing surface with an ϵ_{abs} of 0.5 at 1000°C would have half the thermal emission of a blackbody at 1000°C . Note that the ϵ_{abs} of a surface can change drastically with temperature if its reflectivity and absorbance change 675 for different wavelengths of light. This is because the spectral composition of blackbody radiation changes with temperature. At the same time, the solar absorptance (α_{sol}) of the surface must be maximized to ensure a high power input into the device.

For a surface to have high α_{sol} and low ϵ_{abs} , it must have a low reflectance
680 and high absorbance in visible wavelengths (where most solar light is located),
and a high reflectance in the near infra-red (NIR) region (where most thermal
emission is located). This is a type of spectrally selective surface. These surfaces
must also remain stable under the high operating temperatures found in ST
systems. The relative importance of high α_{sol} and low ϵ_{abs} can change due
685 to changes in system parameters. For example, higher operating temperatures
increase thermal emission and place more importance on achieving a low ϵ_{abs} ,
while higher solar concentrations result in achieving a high α_{sol} being more
important.

Spectrally-selective surfaces are much studied in ST research because they
690 can lead to high-efficiency systems. While coatings for lower ($<500^{\circ}\text{C}$) temper-
atures have been extensively studied, they are generally not suitable for high
temperature operation due to a lack of thermal stability [116]. Some research
has attempted to use silicon or germanium based absorbers, but their high so-
lar reflectance necessitates the use of broad-band anti-reflective coatings which
695 results in high ϵ_{abs} , and their performance degrades at high temperatures due
to oxidation [117].

Stacks of layered dielectric and metallic films can be used to control the
reflectance of structures via multiple reflections and interference effects [118].
Many different materials have been investigated for this purpose, including
700 stacks using tungsten, molybdenum, titanium oxide, and magnesium fluoride
that had an $\epsilon_{abs} < 7\%$ and $\alpha_{sol} > 94\%$ [119, 120, 117]. Unfortunately, fabrica-
tion of these surfaces requires vacuum deposition of multiple layers with precise
thickness, which can be difficult.

Ceramic-metal composites (cermets) consist of metallic particles in a dielec-
705 tric host that are often used as spectrally selective surfaces in ST applications.
The metallic particles in the cermet layer result in high α_{sol} due to multiple
reflections, and they are typically used on metallic substrates with high IR
reflectance, resulting in low ϵ_{abs} [117, 121, 122, 123, 124, 125, 126, 127]. The
disadvantages of cermets include sensitivity to oxygen at high temperatures and

710 the requirement for vacuum fabrication methods.

Nanotextured surfaces can be stable at high temperatures when they are formed from high melting point metals such as tungsten and tantalum and are coated with a protective oxide [43]. They also lend themselves to fabrication using the methods described in this report. Because these methods take advantage of surface geometry, they do not require multiple materials, resulting in a high thermal stability. Indeed, nanostructures of tungsten coated with a protective hafnium coating have been shown to be stable to temperatures of 1100 °C in air [43, 128]. Tantalum photonic crystals have also been reported to be stable at temperatures of over 1000°C [129].

720 Periodic sub-wavelength gratings on tungsten substrates have been fabricated with an α_{sol} of 82% and ϵ_{abs} of 5.6% at 770°C and were experimentally verified to be stable up to temperatures of 900 °C [64]. These structures cause standing wave resonances that can be tuned for solar absorption.

Sub-wavelength roughness on metallic substrates can also increase solar absorption due to the surface acting as a graded index medium [64, 130]. The ϵ_{abs} of these surfaces can be kept low because NIR wavelengths are much longer than the dimensions of the roughness, so the surface appears smooth [131]. An advantage of these types of structures is that they do not require periodicity, and randomness can in fact be an advantage [49]. Simulations have shown pseudo-random nanocones on a tungsten substrate to have an α_{sol} of 97% and ϵ_{abs} of 16% at 1400 °C [49]. Experimental data on surface roughness created by laser-sintering of nanoparticles have shown an α_{sol} of 83% and ϵ_{abs} of 11.6% [29].

4.2. Solar thermophotovoltaics

735 Typical STPV systems consist of an absorbing/emitting structure that is held under vacuum to reduce convective losses and increase thermal stability [41, 132]. Then, sunlight is focused on the absorbing surface of the structure, where it is absorbed and converted into thermal energy. This results in the absorbing/emitting structure becoming very hot, with temperatures up to 1750 K

740 common in these systems. As the system temperature rises, it begins to emit a large amount of thermal radiation. The portion of thermal energy that is emitted by the emitting surface can then be collected by a PV cell and converted into electrical energy. An additional advantage of STPV systems is their ability to store absorbed energy as heat, which is more efficient than battery storage
745 with traditional PV cells. STPV technology can also be easily adapted to thermophotovoltaic (TPV) systems, which operate similarly but use a burning fuel or waste heat as a thermal source instead of the sun.

By transforming the incoming solar radiation from a broad-band source to a more narrow-band one, STPV systems can operate at efficiencies far exceeding
750 the efficiency limit of 29% for single-junction silicon PV cells [133], or the higher limit of 40.8% for a single-junction PV cell with an optimized bandgap [134]. This is due to the fact that the major factors that limit efficiencies in these systems are losses due to below-bandgap radiation and thermalization, which are both dependent on the spectrum of light illuminating the PV cell [135].
755 By efficiently altering the spectrum of light reaching the PV cell, the system efficiency can be increased. In fact, the upper *theoretical* limit for STPV system efficiency is 85.4% [128]. While reference [11] and [41] used many idealities, they clearly show that STPV systems are capable of having efficiencies above the 40.8% limit for single junction PV cells. Detailed balance calculations support
760 this conclusion as well [5].

The absorbing surfaces for STPV devices are similar to those used in ST systems, although higher operating temperatures (up to around 1750 K) make thermal stability a more prominent concern, and high levels of solar concentration (>4000) make a high α_{sol} of paramount concern. This means that
765 nanotextured absorbing surfaces are a very good match for these systems. Most experimental STPV systems to date have utilized blackbody absorbing surfaces [139, 140, 138, 137], leaving room for much improvement by using selective absorbing surfaces. Recent results have reported record efficiencies [19, 90] using both selective absorbers and selective emitters. A yttria-stabilized zirconia and
770 tungsten stack was used as a selective absorber in an experimental system [90],

Table 1: Absorber efficiency corresponding to equation 3, relative solar absorption, and relative thermal emission. These data correspond to a temperature of 1700 K and a concentration factor of 2500 for selected absorbing surfaces.

Absorber type	Absorber efficiency	α_{sol}	ϵ_{abs}
Ideal solar absorber	0.83	0.87	0.04
Pseudo random nano-cones in W	0.80	0.97	0.16 [49]
W pyramidal nanostructures	0.79	0.92	0.13 [74]
Mo-SiO ₂ cermet	0.77	0.93	0.16 [136]
Carbon nanotubes	0.74	0.99	0.95 [137, 18]
1-D photonic crystal on W	0.74	0.80	0.06 [90]
Blackbody absorber	0.73	1.00	1.00
Anti-reflection coating on W	0.67	0.73	0.05 [90]
W cavities	0.59	0.74	0.15 [138]
Surface-relief grating on W	0.49	0.53	0.05 [50]
Bare W	0.41	0.44	0.04 [44]

but while it's thermal emission was low, its performance was hindered by a low α_{sol} of 80%. Simulations of various surfaces have shown large gains in system efficiency from the use of nanotextured selective, such as pseudo-random nanocones with an α_{sol} of 97% and ϵ_{abs} of 16% [49], or pyramidal nanostructures in tungsten with an α_{sol} of 92% and ϵ_{abs} of 13% [74] but none have been
775 experimentally demonstrated in a working STPV system to date.

Various methods of evaluating STPV system performance exist, but in this work we will focus on the relative efficiencies of the individual surfaces of an STPV device. This allows us to directly compare different methods of making
780 selective absorbing and emitting surfaces. Many parameters in STPV systems can effect the performance of these surfaces, so an operating temperature of 1450°C, a solar concentration of 2500, and a GaSb solar cell are assumed here due to their prevalence in STPV systems [139, 140, 138, 49, 54, 11]. This provides for a good relative comparison of different surfaces, although it is not
785 a measure of overall device efficiency.

Table 1 shows the α_{sol} and ϵ_{abs} of some absorbing surfaces, as well as a calculated surface efficiency. The quantity η_{abs} is given by

$$\eta_{abs}(T) = \frac{\int_0^\infty \{E_{inc}(\lambda)\alpha(\lambda) - \epsilon(\lambda)B(\lambda, T)\} d\lambda}{\int_0^\infty E_{inc}(\lambda) d\lambda} \quad (3)$$

$$E_{inc}(\lambda) = C E_{sun}(\lambda), \quad (4)$$

where $\alpha(\lambda)$ is the spectral absorption of the surface, $\epsilon(\lambda)$ is the spectral emittance of the surface, C is the concentration factor of incoming sunlight, including concentrator ratio and concentrator efficiency, $E_{sun}(\lambda)$ is the spectral irradiance of the sun at the earth's surface, $B(\lambda, T)$ is Planck's law for blackbody radiation,
790 and $E_{inc}(\lambda)$ is the spectral energy incident on the absorbing surface.

For emitting surfaces, a similar approach to absorbing surfaces can be taken, but with a focus on low reflectance in a narrow peak near a specific wavelength (which depends on the bandgap energy of the PV cell used), as opposed to a broad low reflectance band in the visible region. To accurately compare emitting
795 surfaces, their ultimate efficiency is used.

The ultimate efficiency is given by [54]:

$$\eta = \frac{\int_0^{\lambda_{bg}} \frac{E_{bg}}{E_\lambda} B(\lambda, T) \epsilon_S(\lambda) d\lambda}{\int_0^\infty B(\lambda, T) \epsilon_S(\lambda) d\lambda} \quad (5)$$

where E_{bg} is the bandgap energy of the PV cell, E_λ is the energy of a photon with wavelength λ , and $\epsilon_S(\lambda)$ is the spectral emissivity of the emitting surface, approximated as the surface's absorptivity. This gives the relative efficiency of the emitting surface, but does not represent an overall system efficiency.

Specifically, this equation does not take into account the fill factor, open-circuit voltage, recombination losses within the PV cell, or any non-idealities in the STPV system. The values obtained from this equation do not represent real or even potential system efficiencies, but serve as a convenient way to compare the performance of various surfaces as well as a tool for optimization. While PV cells with external quantum efficiencies that vary by wavelength could change the optimum bandgap stated by this equation, the effect is generally small and would need to be evaluated on a case by case basis. We note that typically, the emissivity of the emitter structure will depend upon angle, and so the angular integration cannot simply be assumed to lead to a constant factor as suggested by Eq. (5) above; see, for example, Ref. [11] for a definition of the emitter efficiency that depends explicitly upon emission angle.

Two structures work particularly well for this purpose: dielectric-metal stacks and 2-D or 3-D photonic crystals. A yttria-stabilized zirconia (YSZ) and tungsten stack was able to achieve highly selective emission and experimentally demonstrated to be stable at temperatures up to 1350 °C [90].

Many nanotextured emitting structures have been simulated to be extremely efficient [51]. These include blazed gratings on tungsten [54], complex square gratings on tungsten [52], micro-cavities in tungsten [42], tungsten surface gratings [50], 3-D photonic crystals [141], and metamaterials [142]. Table 2 shows the ultimate efficiencies of some of these surfaces. This shows a large increase in efficiency for selective emitters over blackbody emitters. While experimental systems using these structures have not yet been realized, they promise large efficiency gains for the future. Table 3 shows the electrical efficiencies of some

Table 2: Ultimate efficiency of selected emitting surfaces at 1700 K and a bandgap of 0.72 eV [39].

Emitter type	η_{emit}
Ideal emitting surface	0.84
Periodic hole array on W	0.64 (simulated)
Blazed grating on W	0.59 [54]
Anti-reflection coating on W	0.59 (simulated)
Complex square grating on W	0.53 [52]
1-D photonic crystal on W	0.53 [90]
Micro-cavity in W	0.51 [42]
Al ₂ O ₃ /Er ₃ Al ₅ O ₁₂ eutectic composite	0.41 [139]
Blackbody emitter	0.29

simulated and experimental STPV systems. These efficiencies are for systems
825 operating under AM1.5 solar simulators or real-world solar conditions. They all
are converting solar energy to usable electrical energy (work).

The simulations outlined here show a large difference in predicted efficiency;
however, a significant portion of this variation is caused by simulation paramet-
ters. Since there is no standard for simulated STPV systems, some papers use
830 an ideal model where only losses due to the surfaces are accounted for, while
others use a more realistic model that encompasses many losses. Namely, refer-
ences [11] and [41] assume ideal PV cells, ideal solar concentrators, and assume
an ideal view-factor between the emitting surface and solar cells. References
[42], [39], and [20] attempt to model PV cell losses and realistic absorbing and
835 emitting surfaces. Some of the remaining difference between efficiencies in the
modeled systems is also due to differences in assumptions between simulations.
Additional technical challenges associated with STPV and TPV systems that
are not included in any of the aforementioned studies include the high resistance
losses associated with large current outputs from PV cells, and the large amount

840 of cooling necessary to hold the PV cells at adequate temperatures. While the use of selective emitters does significantly reduce the thermal load on the PV cells, active cooling will still be necessary for systems which utilize a high level of solar concentration. The power required for this cooling is not taken into account in the efficiency numbers outlined in this review.

845 Despite the assumptions in these models, they show that nanostructured surfaces are extremely important to ensure adequate spectral selectivity in these systems. References [42], [39], and [20] predict high potential operating efficiencies using realistic operating conditions. The primary reason that experimental systems lag behind simulations is because a lack of high quality nanostructures
850 in these systems [90, 143]. The YSZ and W stack used in [90] proved to be a less efficient solution for both the absorbing and emitting surfaces than other surfaces examined in this article. In [143], secondary, less efficient surfaces had to be used for both the absorbing and emitting structures due to fabrication problems. References [90, 137, 18] uses a blackbody absorbing surface, which
855 results in suboptimal efficiency. Still, these devices are able to achieve very high operating efficiencies by operating at low temperatures to mitigate thermal emission from the absorber and by using nanostructured emitting surfaces. The inclusion of an extra filter on emitted light to reduce losses in the emitting surface can also increase efficiency[18]. Still, theoretical efficiencies are much
860 higher than experimental ones. This points to a large increase in efficiency that can be achieved by using nanostructures to close the gap between experimental and theoretical devices. The simulation and fabrication methods outlined in this paper show that this is possible.

Thermophotovoltaic (TPV) systems are another important area for harvest-
865 ing waste heat energy. The reported efficiency of TPV systems is low at around few percent. However, as demonstrated by Bermel et al. [4] by using spectral selective surfaces the calculated efficiency can be very high (26.2%). The calculation was based on operating temperature of 1200°C. Similarly, Foley et al. [77] has shown in the paper as part of this special issue that by using metal (Ag)-
870 dielectric (Si_3N_4) structure the calculated efficiency of 10% can be achieved at

Table 3: Efficiency of selected STPV systems. A_{ratio} refers area of the emitter divided by area of the absorber. C refers to concentration factor of the incident solar radiation.

Absorbing surface	Emitting surface	PV cell	T (K)	C	A_{ratio}	Efficiency (%)
Experimental systems						
YSZ and W stack	YSZ and W stack	GaSb	1640	450	1	8 [90]
Carbon nanotubes	Si/SiO ₂ stack	InGaAsSb	1200	100	12	6.8 [18]
Laser-textured W	W with Si ₃ N ₄	GaSb	1777	2500	10	6.2 [143]
with Si ₃ N ₄ coating	coating					
Carbon nanotubes	Si/SiO ₂ stack	InGaAsSb	1285	750	7	3.2 [137]
Tungsten cavity	Thin W film	GaSb	~2000	770	5.7	1 [138]
Graphite	W with HfO ₂	Ge	~1700	900	10	0.8 [140]
	coating					
Graphite	Al ₂ O ₃ /Er ₃ Al ₅ O ₁₂	GaSb	N/A	25000	0.27	0.02 [139]
	composite					
Simulated systems						
Pyramidal W	Si/SiO ₂ stack	GaSb	2130	20000	100	49 [11]
nanostructures						
Blackbody absorber	Monochromatic	Ideal cell	2872	46050	100	45.3 [41]
	emitter					
Selective absorber	W surface grating	GaSb	1920	5000	10	23.4 [42]
	with Si/SiO ₂ filter					
Periodic hole	Pseudo-random	GaSb	1700	2500	10	14.4 [39]
array on W	cones on W					
2D Ta photonic	2D Ta photonic	InGaAsSb	1400	18000	1	10 [20]
crystal	crystal					

low operating temperature of 1000°C. It can also be further enhanced by using selective filters and operating at 1200°C.

5. Conclusions

We discussed a variety of modeling and fabrication techniques for controlling
875 light absorption and emission by nanostructures. Such control is important for
solar and thermal energy conversion devices including traditional photovoltaic
(PV), solar thermal (ST), and solar thermophotovoltaic (STPV) devices. The
use of thermal energy conversion in particular, can circumvent some efficiency
limitations on standard PV cells. We anticipate that significant efficiency im-
880 provements can be achieved in this area by building on the techniques discussed
here. For example, while ST systems are already achieving high efficiencies
in commercial use, experimental TPV and STPV efficiencies remain low. The
primary cause of lowered device efficiency is lack of control over the spectral
emissivity of the absorbing and emitting surfaces. The nanostructures, simula-
885 tion, and fabrication methods highlighted here can be used to greatly increase
efficiencies in all three of these systems. Indeed, simulations of nanostructured
devices show that extremely high efficiencies are achievable in TPV/STPV sys-
tems. For example, one of the most promising simulated devices have shown
conversion efficiencies of 26.2% at system temperatures of 1200°C and a max-
890 imum conversion efficiency of 49% was predicted for system temperatures of
about 2130 K [11]. However, the highest conversion efficiency measured for
an STPV device is about 8% for 1D photonic crystal structures composed of
tungsten and YSZ at device temperatures of 1640 K [90]. This large gap in sys-
tem efficiency is due to the lack of temperature-stable nanostructures and high
895 losses in experimental STPV systems. Future theoretical design methodologies
should involve explicit considerations of aspects like thermal properties of ma-
terials and the thermal deformation of nanostructures to guide the fabrication
of structures that are more robust to thermal degradation. Additional thermal
management strategies including the use of ST systems in tandem with STPV

900 systems to capture waste heat from the STPV device should be explored.

Acknowledgments

We would like to thank the NASA Langley Professor and NSF IUCRC programs for their support of this project. Part of this work was performed at the Center for Nanoscale Materials, a U.S. Department of Energy, Office of Science,
905 Office of Basic Energy Sciences User Facility under Contract No. DE-AC02-06CH11357. JJF acknowledges the Center for Research at William Paterson University for financial support.

References

- [1] M. Thirugnanasambandam, S. Iniyar, R. Goic, A review of solar thermal
910 technologies, *Renewable and Sustainable Energy Reviews* 14 (2010) 312–322.
- [2] Y. Tian, C. Y. Zhao, A review of solar collectors and thermal energy storage in solar thermal applications, *Applied Energy* 104 (2013) 538–553.
- [3] T. Bauer, *Thermophotovoltaics: basic principles and critical aspects of system design*, Springer, 2011.
915
- [4] P. Bermel, M. Ghebrebrhan, W. Chan, Y. X. Yeng, M. Araghchini, R. Hamam, C. H. Marton, K. F. Jensen, M. Soljacic, J. D. Joannopoulos, S. G. Johnson, I. Celanovic, Design and global optimization of high-efficiency thermophotovoltaic systems, *Opt. Express* 18 (2010) A314–334.
- 920 [5] N. Harder, P. Wurfel, Theoretical limits of thermophotovoltaic solar energy conversion, *Semiconductor Science and Technology* 18 (2003) S151.
- [6] O. Dupre, R. Vaillon, M. A. Green, Optimization of solar thermophotovoltaic systems including the thermal balance, *Proc. of the 43rd IEEE PVSC*.

- 925 [7] C. Ferrari, F. Melino, M. Pinelli, P. R. Spina, M. Venturini, Overview and
status of thermophotovoltaic systems, *Energy Procedia* 45 (2014) 1160–
1169.
- [8] P. Bermel, J. Lee, J. D. Joannopoulos, I. Celanovic, M. Soljacic, Selective
solar absorbers, *Annual Review of Heat Transfer*, Begell House Inc., 2012,
930 Ch. 7.
- [9] T. Inoue, M. Zoysa, T. Asano, S. Noda, Realization of narrowband thermal
emission with optical nanostructures, *Optica* 2 (2015) 27.
- [10] A. Lenert, D. M. Bierman, Y. Nam, W. R. Chan, I. Celanovic, M. Sol-
jadic, E. N. Wang, A nanophotonic solar thermophotovoltaic device, *Nat.*
935 *Nanotechnol.* 9 (2014) 126–130.
- [11] E. Rephaeli, S. Fan, Absorber and emitter for solar thermophotovoltaic
systems to achieve efficiency exceeding the schockley-queisser limit, *Opt.*
Express 17 (2009) 15145–15159.
- [12] C. G. Granqvist, Spectrally selective coatings for energy efficiency and
940 solar applications, *Phys. Scripta* 32 (1985) 401.
- [13] S. Collin, Nanostructure arrays in free space: optical properties and ap-
plications, *Rep. Prog. Phys.* 77 (2014) 126402.
- [14] A. Datas, D. L. Chbb, A. Veeraragavan, Steady state analysis of a storage
integrated solar thermophotovoltaic (sistpv) system, *Sol. Energy* 96 (2013)
945 33–45.
- [15] A. Veeraragavan, L. Montgomery, A. Datas, Night time performance of a
storage intergrated solar thermophotovoltaic (sistpv) system, *Sol. Energy*
108 (2014) 377–389.
- [16] W. Durisch, B. Bitnar, F. von Roth, G. Palfinger, Small thermophoto-
950 voltaic prototype systems, *Sol. Energy* 75 (2003) 11–15.

- [17] V. S. Reddy, S. C. Kaushik, K. R. Ranjan, S. K. Tyagi, State-of-the-art of solar thermal power plants-a review, *Renew. Sust. Energ. Rev.* 27 (2013) 258–273.
- [18] D. M. Blerman, A. J. Lenert, W. R. Chan, B. Bhatka, I. Celanovic, M. Soljagic, E. N. Wang, Enhanced photovoltaic energy conversion using thermally based spectral shaping, *Nat. Enrgy.* 1 (2016) 1–7.
- [19] V. Rinnerbauer, A. Lenert, D. M. Bierman, Y. X. Yeng, W. R. Chan, R. D. Geil, J. J. Senkevich, J. D. Joannopoulos, E. N. Wang, M. Soljagic, I. Cleanovic, Metallic photonic crystal absorber-emitter for efficient spectral control in high-temperature solar thermophotovoltaics, *Advanced Energy Materials* 4 (2014) 1400334.
- [20] Y. Nam, Y. X. Yeng, A. Lenert, P. Bermel, I. Celanovic, M. Soljačić, E. N. Wang, Solar thermophotovoltaic energy conversion systems with two-dimensional tantalum photonic crystal absorbers and emitters, *Sol. Energy Mat. Sol. Cells* 122 (2014) 287 – 296.
- [21] V. Stelmakh, V. Rinnerbauer, W. R. Chan, J. J. Senkevich, J. D. Joannopoulos, M. Soljagic, I. Celanovic, Tantalum-tungsten alloy photonic crystals for high-temperature energy conversion systems, *Proceedings of the SPIE - The International Society for Optical Engineering* 9127 (2014) 91270Q.
- [22] I. Celanovic, N. Jovanovic, J. Kassakian, Two-dimensional tungsten photonic crystals as selective thermal emitters, *Appl. Phys. Lett.* 92 (2008) 193101.
- [23] H. Wang, V. P. Sivan, A. Mitchell, G. Rosengarten, P. Phelan, L. Wan, Highly efficient selective metamaterial absorber for high-temperature solar thermal energy harvesting, *Sol. Energy Mat. Sol. Cells* 137 (2015) 235–242.
- [24] X. Liu, T. Tyler, T. Starr, A. Starr, N. Jokerst, W. Padilla, Taming

the blackbody with infrared metamaterials as selective thermal emitters,
 Phys. Rev. Lett. 107 (2011) 045901.

- 980 [25] I. Khodasevich, L. Wang, A. Mitchell, G. Rosengarten, Micro and nanos-
 structured surfaces for selective solar absorption, Adv. Opt. Mater. 107
 (2015) 045901, doi: 10.1002/adom.201500063.
- [26] Y. Son, J. Yeo, C. Woo, H. Sukjoon, H. Seung, H. Ko, D. Yang, Fabrica-
 tion of submicron-sized metal patterns on a flexible polymer substrate by
 985 femtosecond laser sintering of metal nanoparticles, International Journal
 of Nanomanufacturing 9 (2013) 468–476.
- [27] E. P. B. Filho, O. S. H. Mendoza, C. L. L. Beicker, A. Menezes, D. Wen,
 Experimental investigation of a silver nanoparticle-based direct absorption
 solar thermal system, Energy Conversion and Management 84 (2014) 261–
 990 267.
- [28] G. Katumba, L. Olumekor, A. Forbes, G. Makiwa, B. Mwakikunga, J. Lu,
 E. Wackelgard, Optical, thermal and structural characteristics of carbon
 nanoparticles embedded in ZnO and NiO as selective solar absorbers, Sol.
 Energy Mater. and Solar Cells 92 (2008) 1285–1292.
- 995 [29] A. A. Shah, M. C. Gupta, Spectral selective surfaces for concentrated solar
 power receivers by laser sintering of tungsten micro and nano particles,
 Sol. Energy Mat. Sol. Cells 117 (2013) 489–493.
- [30] J. H. Schon, G. Binder, E. Bucher, Performance and stability of some new
 high-temperature selective absorber systems based on metal/dielectric
 1000 multilayers, Sol. Energy Mat. Sol. Cells 33 (1994) 403–416.
- [31] V. K. Narasimhan, Y. Cui, Nanostructures for photon management in
 solar cells, Nanophotonics 2 (2013) 187210.
- [32] M. C. Gupta, B. K. Nayak, V. Iyengar, L. Wang, Efficient light trapping
 by laser microtexturing of surfaces for photovoltaics, SPIE NewsroomDOI:
 1005 10.1117/2.1201208.004361.

- [33] M. C. Gupta, D. E. Carlson, Laser processing for renewable energy materials, *MRS Energy and Sustainability: A Review Journal*-DOI:10.1557/mre.2015.3.
- 1010 [34] V. V. Iyengar, B. K. Nayak, M. C. Gupta, Ultralow reflectance metal surfaces by ultrafast laser texturing, *Appl. Opt.* 49 (2010) 5983–5988.
- [35] A. Luque, Solar thermophotovoltaics: Combining solar thermal and photovoltaics, *AIP Conf. Proc.* 890 (1) (2007) 3–16.
- 1015 [36] J. L. Duomarco, R. Kaplow, Theoretical estimations of the efficiency of thermophotovoltaic systems using high-intensity silicon solar cells, *Sol. Energy* 32 (1984) 33–40.
- [37] A. Luque, Solar thermophotovoltaics: combining solar thermal and photovoltaics, *AIP Conference Proceedings* 3 (2007) 3–16.
- [38] P. Gleckman, J. O’Gallagher, R. Winston, Concentration of sunlight to solar-surface levels using non-imaging optics, *Nature* 339 (1989) 198–200.
- 1020 [39] C. Ungaro, Control of optical properties of surfaces for improved solar thermophotovoltaic systems, Phd thesis, University of Virginia (2015).
- [40] R. K. McGovern, W. J. Smith, Optimal concentration and temperatures of solar thermal power plants, *Energy Convers. Manage.* 60 (2012) 226–232.
- 1025 [41] A. Datas, C. Algora, Global optimization of solar thermophotovoltaic systems, *Progress in Photovoltaics: Research and Applications* 21 (2013) 1040–1055.
- [42] Y. Xuan, X. Chen, Y. Han, Design and analysis of thermophotovoltaic systems, *Renew. Energy*. 36 (2011) 374–387.
- 1030 [43] K. A. Arpin, M. D. Losego, P. V. Braun, Electrodeposited 3D tungsten photonic crystals with enhanced thermal stability, *Chemistry of Materials* 23 (2011) 4783–4788.

- [44] E. D. Palik, Handbook of optical constants of solids, Academic Press, 1998.
- [45] T. K. Chaudhuri, A solar thermophotovoltaic converter using pbs photo-
1035 voltaic cells, Int. J. Energy Res 16 (1992) 481–487.
- [46] A. Azens, M. Kitenbergs, U. Kandars, Evaporation of tungsten oxides: A
mass-spectrometric study of vapour contents, Vacuum 46 (1995) 745–747.
- [47] D. MacIsaac, G. Kanner, G. Anderson, Basic physics of the incandescent
lamp (lightbulb), Phys. Teach. 37 (1999) 520.
- 1040 [48] M. Shimizu, A. Kohiyama, H. Yugami, High-efficiency solar ther-
mophotovoltaic system equipped with a monolithic planar selective ab-
sorber/emitter, J. Photon. Energy 5 (2015) 053099.
- [49] C. Ungaro, S. K. Gray, M. C. Gupta, Black tungsten for solar power
generation, Appl. Phys. Lett. 103 (7) (2013) 071105–071105–3.
- 1045 [50] H. Sai, H. Yugami, Thermophotovoltaic generation with selective radiators
based on tungsten surface gratings, Appl. Phys. Lett. 85 (2004) 3399–3401.
- [51] H. Sai, Y. Kanamori, K. Hane, H. Yugami, M. Yamaguchi, Numerical
study on tungsten selective radiators with various micro/nano structures,
Photovoltaic Specialists Conference (2005) 762–765.
- 1050 [52] Y. B. Chen, Z. M. Zhang, Design of tungsten complex gratings for ther-
mophotovoltaic radiators, Opt. Comm. 269 (2007) 411–417.
- [53] E. B. Grann, M. G. Moharam, Comparison between continuous and dis-
crete subwavelength grating structures for antireflection surfaces, J. Opt.
Soc. Am. 13 (1996) 988–922.
- 1055 [54] C. Ungaro, S. K. Gray, M. C. Gupta, Graded-index structures for high-
efficiency solar thermophotovoltaic emitting surfaces, Opt. Lett. 39 (18)
(2014) 5259–5262.

- [55] S. K. Gray, Theory and modeling of plasmonic structures, *J. Phys. Chem. C* 117 (2013) 1983–1994.
- 1060 [56] A. Taflove, S. C. Hagness, *Computational Electrodynamics: the finite-difference time-domain method*, Artech, 2000.
- [57] A. F. Oskooi, D. Roundy, M. Ibanescu, P. Bermel, J. D. Joannopoulos, S. G. Johnson, Meep: A flexible free-software package for electromagnetic simulations by the FDTD method, *Comp. Phys. Comm.* 181 (2010) 687702.
- 1065 [58] C. F. Bohren, D. R. Huffman, *Absorption and Scattering of Light by Small Particles*, John Wiley and Sons, 1998.
- [59] P. Yeh, *Optical waves in layered media*, Wiley, 2005.
- [60] B. T. Draine, P. J. Flatau, Discrete-dipole approximation for scattering calculations, *J. Opt. Soc. Am. A* 11 (1994) 1491–1499.
- 1070 [61] J. M. McMahon, Topics in theoretical and computational nanoscience: From controlling light at the nanoscale to calculating quantum effects with classical electrodynamics, Ph.D. thesis, Northwestern University (2011).
- [62] M. G. Moharam, D. A. Pommet, E. B. Grann, T. K. Gaylor, Stable implementation of the rigorous coupled-wave analysis for surface-relief gratings: enhanced transmittance matrix approach, *J. Opt. Soc. A* 12 (1995) 1077.
- 1075 [63] L.-L. Lin, Z.-Y. Li, K.-M. Ho, Lattice symmetry applied in transfer-matrix methods for photonic crystals, *J. Appl. Phys.* 98 (2003) 811.
- [64] H. Saia, H. Yugamia, Y. Kanamori, K. Hane, Solar selective absorbers based on two-dimensional W surface gratings with submicron periods for high-temperature photothermal conversion, *Sol. Energy Mat. Sol. Cells* 79 (2003) 35–49.
- 1080

- [65] V. Rinnerbauer, Y. Shen, J. D. Joannopoulos, M. Soljaic, F. Schaffler, I. Celanovic, Superlattice photonic crystal as broadband solar absorber for high temperature operation, *Opt. Express* 22 (2014) A1895.
- [66] R. G. Barrerra, M. del Castillo-Mussot, G. Monsivais, P. Villaseor, W. L. Mochán, Optical properties of two-dimensional disordered systems on a substrate, *Phys. Rev. B* 38 (1988) 5371.
- [67] R. G. Barrerra, G. Monsivais, W. L. Mochán, Renormalized polarizability in the maxwel garnett theory, *Phys. Rev. B* 43 (1991) 13819.
- [68] S. Yoo, Q.-H. Park, Effective permittivity for resonant plasmonic nanoparticle systems via dressed polarizability, *Opt. Express* 20 (2012) 16480.
- [69] H. A. Atwater, A. Polman, Plasmonics for improved photovoltaic devices, *Nature Mater.* 9 (2010) 205–213.
- [70] J. M. Geffrin, B. García-Cámara, R. Gómez-Medina, P. Albella, L. S. Froufe-Pérez, C. Eyraud, A. Litman, R. Vaillon, F. González, M. Nieto-Vesperinas, J. J. Sáenz, F. Moreno, Magnetic and electric coherence in forward- and back-scattered electromagnetic waves by a single dielectric subwavelength sphere, *Nat. Commun.* 3 (2012) 1171.
- [71] J. R. Cole, N. J. Halas, Optimized plasmonic nanoparticle distributions for solar spectrum harvesting, *Appl. Phys. Lett.* 89 (2006) 153120.
- [72] K. T. Fountaine, C. G. Kendall, H. A. Atwater, Near-unity broadband absorption designs for semiconducting nanowire arrays via localized radial mode excitation, *Opt. Express* 22 (2014) A930.
- [73] P. Spinelli, M. A. Verschuuren, A. Polman, Broadband omnidirectional antireflection coating based on subwavelength surface Mie resonators, *Nat. Commun.* 3 (2012) 692.
- [74] E. Rephaeli, S. Fan, Tungsten black absorber for solar light with wide angular operation range, *Appl. Phys. Lett.* 92 (2008) 211107.

- 1110 [75] P. Ben-Adballah, B. Ni, Single-defect bragg stacks for high-power narrow-band thermal emission, *J. Appl. Phys* 97 (2005) 104910.
- [76] B. J. Lee, Z. M. Zhang, Design and fabrication of planar multilayer structures with coherent thermal emission characteristics, *J. Appl. Phys* 100 (2006) 063529.
- 1115 [77] J. J. Foley IV, C. Ungaro, K. Sun, M. C. Gupta, S. K. Gray, Design of emitter structures based on resonant perfect absorption for thermophotovoltaic applications, *Opt. Express* 23 (2015) A1373.
- [78] J. J. Foley IV, J. M. McMahon, G. C. Schatz, H. Harutyunyan, G. P. Wiederrecht, S. K. Gray, Inhomogeneous surface plasmon polaritons, *ACS Photonics* 1 (2014) 739–745.
- 1120 [79] P. C. Chang, J. G. Walker, K. I. Hopcraft, Ray tracing in absorbing media, *J. Quant. Spectrosc. Radiat. Transfer* 96 (2005) 327–341.
- [80] L. Wendler, R. Haupt, An improved virtual mode theory of ATR experiments of surface polaritons, *Phys. Stat. Sol. b* 143 (1987) 131–147.
- 1125 [81] S. M. Maier, *Plasmonics: Fundamentals and applications*, Springer, 2007.
- [82] L. Novotny, B. Hecht, *Principles of nano-optics*, 2nd Edition, Cambridge University Press, 2012.
- [83] J. J. Foley IV, H. Harutyunyan, D. Rosenmann, R. Divan, G. P. Wiederrecht, S. K. Gray, When are surface plasmon polaritons excited in the Kretschmann-Raether configuration?, *Sci. Rep.* 5 (2015) 09929.
- 1130 [84] E. F. C. Driessen, M. J. A. de Dood, The perfect absorber, *Appl. Phys. Lett.* 94 (2009) 171109.
- [85] M. A. Kats, D. Sharma, J. Lin, P. Genevet, R. Blanchard, Z. Yang, M. M. Qazilbash, D. N. Basov, S. Ramanathan, F. Capasso, Ultra-thin perfect absorber employing a tunable phase change material, *App. Phys. Lett.* 101 (2012) 221101.
- 1135

- [86] M. A. Kats, R. Blachard, P. Genevet, F. Capasso, Nanometer optical coatings based on strong interference effects in highly absorbing media, Nat. Mat. 12 (2013) 20–24.
- 1140 [87] H. Raether, Surface Plasmons on Smooth and Rough Surfaces and on Gratings, Springer-Verlag, 1988.
- [88] J. Drevillon, P. Ben-Abdallah, *Ab initio* design of coherent thermal sources, J. Appl. Phys. 102 (2007) 114305.
- 1145 [89] E. Nefzaoui, J. Drevillon, K. Joulain, Selective emitters design and optimization for thermophotovoltaic applications, J. Appl. Phys. 111 (2012) 084316.
- [90] M. Shimizu, A. Kohiyama, H. Y. Yugami, High-efficiency solar-thermophotovoltaic system equipped with a monolithic planar selective absorber/emitter, J. Photon. Energy 5 (2015) 053099–53107.
- 1150 [91] A. Karalis, J. D. Joannopoulos, ‘squeezing’ near-field thermal emission for ultra-efficient high-power thermophotovoltaic conversion, Sci. Rep. 6 (2016) 28472.
- [92] A. W. Rodriguez, O. Ilic, P. Bermel, I. Celanovic, J. D. Joannopoulos, M. Soljacic, S. G. Johnson, Frequency-selective near-field radiative heat transfer between photonic crystal slabs: A computational approach for arbitrary geometries and materials, Phys. Rev. Lett. 107 (2011) 114302.
- 1155 [93] A. Datas, D. Hirashima, K. Hanamura, FDTD simulation of near-field radiative heat transfer between thin films supporting surface phonon polaritons: Lessons learned, J. Therm. Sci. Tech. 8 (2013) 91–105.
- 1160 [94] A. Didari, M. P. Menguc, Analysis of near-field radiation transfer within nano-gaps using FDTD method, J. Quant. Spect. Radiat. Transf. 146 (2014) 214–226.

- [95] A. Didari, M. P. Menguc, Near-field thermal emission between corrugated surfaces separated by nano-gaps, *J. Quant. Spect. Radiat. Transf.* 158 (2015) 43–51.
- [96] R. St-Gelais, L. Zhu, S. Fan, M. Lipson, Near-field radiative heat transfer between parallel structures in the deep subwavelength regime, *Nat. Nano.* 11 (2016) 515–519.
- [97] K. Aydin, V. E. Ferry, R. M. Briggs, H. A. Atwater, Broadband polarization-independent resonant light absorption using ultrathin plasmonic super absorbers, *Nature Comm.* 2 (2011) 517.
- [98] Lumerical Solutions, Inc., <http://www.lumerical.com/tcad-products/mode/>.
- [99] M. A. Yurkin, M. Min, A. G. Hoekstra, Application of the discrete dipole approximation to very large refractive indices: Filtered coupled dipoles revived, *Phys. Rev. E* 82 (2010) 036703.
- [100] V. L. Y. Loke, M. P. Menguc, Surface waves and atomic force microscope probe-particle near-field coupling: discrete dipole approximation with surface interaction, *J. Opt. Soc. Am. A* 27 (2010) 2293–2303.
- [101] S. Edalatpour, M. Francoeur, The thermal discrete dipole approximation (t-dda) for near-field radiative heat transfer simulations in three-dimensional arbitrary geometries, *J. Quant. Spect. Radiat. Transf.* 133 (2015) 364–373.
- [102] J. A. Nelder, R. Mead, A simplex method for function minimization, *Comp. J.* 7 (1965) 308–313.
- [103] A. Lin, J. Phillips, Optimization of random diffraction gratings in thin-film solar cells using genetic algorithms, *Sol. Energy Mat. Sol. Cells* 92 (2008) 1689–1696.
- [104] M. Clerc, *Particle Swarm Optimization*, Wiley, 2008.

- 1190 [105] R. L. Miller, Z. Xie, S. Leyffer, M. J. Davis, S. K. Gray, Surrogate-based modeling of the optical response of metallic nanostructures, *J. Phys. Chem. C* 114 (2010) 20741–20748.
- [106] M. Elzouka, S. Ndao, Towards a near-field concentrated solar thermophotovoltaic microsystem: Part i - modeling, *Sol. Energy* 141 (2017) 323–333.
- 1195 [107] M. P. Bernardi, O. Dupré, E. Blandre, P.-O. Chapuis, R. Vaillon, M. Francoeur, Impacts of propagating, frustrated and surface modes on radiative, electrical and thermal losses in nanoscale-gap thermophotovoltaic power generators, *Sci. Rep* 5 (2015) 11626.
- [108] V. V. Iyengar, B. K. Nayak, M. C. Gupta, Optical characteristics of femtosecond laser micromachined periodic structures in Si 100, *Appl. Opt.* 45
1200 (2006) 7137–7143.
- [109] M. C. Gupta, S. T. Peng, Diffraction characteristics of surface-relief gratings, *Appl. Opt.* 32 (1993) 2911–2917.
- [110] W. M. Steen, J. Mazumder, *Laser Material Processing*, 4th Edition,
1205 Springer, 2010.
- [111] M. M. Hawkeye, M. T. Tashuk, M. J. Brett, *Glancing Angle Deposition of Thin Films: Engineering the Nanoscale*, Wiley, 2014.
- [112] C. Ungaro, A. Shah, I. Kravchenko, D. K. Hensley, S. K. Gray, M. C. Gupta, Optical and infrared properties of glancing angle deposited nanostructured tungsten films, *Opt. Lett.* 40 (2015) 506–509.
1210
- [113] Schott Solar CSP GmbH, http://www.schott.com/d/csp/2ad9cb93-5b86-4a51-aead-a49b4e869ef8/1.0/schott_ptr70_4th_generation_datasheet.pdf.
- [114] Y. You, E. J. Hu, A medium-temperature solar thermal power system and
1215 its efficiency optimisation, *Appl. Therm. Eng.* 22 (2002) 357–364.

- [115] C. K. Ho, B. D. Iverson, Review of high-temperature central receiver designs for concentrating solar power, *Renew. Sustainable Energy Rev.* 29 (2014) 835–846.
- 1220 [116] N. Selvakumar, H. Barshilia, Review of physical vapor deposited (pvd) spectrally selective coatings for mid- and high-temperature solar thermal applications, *Sol. Energy Mat. Sol. Cells* 98 (2012) 1–23.
- [117] C. E. Kennedy, Review of mid-to-high temperature solar selective absorber materials. technical report nrel/tp-520-31267, Tech. rep., National Renew. Energ. Laboratory (2002).
- 1225 [118] X. Li, Y. Chen, J. Miao, P. Zhou, Y. Zheng, L. Chen, High solar absorption of a multilayered thin film structure, *Opt. Express* 15 (2007) 1907–1912.
- [119] N. P. Sergeant, O. Pincon, M. Agrawal, P. Peumans, Design of wide-angle solar-selective absorbers using aperiodic metal-dielectric stacks, *Opt. Express* 17 (2009) 22800–22812.
- 1230 [120] N. P. Sergeant, M. Agrawal, P. Peumans, High performance solar-selective absorbers using coated sub-wavelength gratings, *Opt. Express* 18 (2010) 5525–5540.
- [121] S. Esposito, A. Antonaia, M. Addonizio, S. Aprea, Fabrication and optimization of highly efficient cermet-based spectrally selective coatings for high operating temperature, *Thin Solid Films* 517 (2009) 6000–6006.
- 1235 [122] L. T. A. Berghaus, A. Djahanbakhsh, Characterisation of cvd - tungsten alumina cermets for high-temperature selective absorbers, *Sol. Energy Mat. Sol. Cells* 54 (1998) 19–26.
- [123] M. Farooq, M. Hutchins, Optical properties of higher and lower refractive index composites in solar selective coatings, *Sol. Energy Mat. Sol. Cells* 71 (2002) 73–83.
- 1240

- [124] D. Xinkang, W. Cong, W. Tianmin, Z. Long, C. Buliang, R. Ning, Microstructure and spectral selectivity of Mo-Al₂O₃ solar selective absorbing coatings after annealing, *Thin Solid Films* 516 (2008) 3971–3977.
- 1245 [125] Q. Zhang, Y. Yin, D. Mills, High efficiency Mo-Al₂O₃ cermet selective surfaces for high-temperature applications, *Sol. Energy Mat. Sol. Cells* 40 (1996) 43–53.
- [126] Q. Zhang, Recent progress in high-temperature solar selective coatings, *Sol. Energy Mat. Sol. Cells* 62 (2000) 63–74.
- 1250 [127] R. Schmidt, K. Park, High-temperature space-stable selective solar absorber coatings, *Appl. Opt.* 4 (1965) 917–925.
- [128] C. Schlemmer, J. Aschaber, V. Boerner, J. Luther, Thermal stability of micro-structured selective tungsten emitters, *Thermophotovoltaic Generation of Electricity: 5th Conference*, CP653 - American Institute of Physics.
- 1255 [129] V. Rinnerbauer, S. Ndao, Y. X. Yeng, W. R. Chan, J. J. Senkevich, J. D. Joannopoulos, M. Soljacic, I. Celanovic, Recent developments in high-temperature photonic crystals for energy conversion, *Energy and Environmental Science*.
- 1260 [130] F. Ghmari, T. Ghbara, M. Laroche, R. Carminati, J.-J. Greffet, Influence of microroughness on emissivity, *Journal of Applied Physics* 96 (2004) 2656–2664.
- [131] A. Lasagni, M. Nejati, R. Clasen, F. Mucklich, Periodical surface structuring of metals by laser interference metallurgy as a new fabrication method of textured solar selective absorbers, *Adv. Eng. Mater.* 8 (2006) 580–584.
- 1265 [132] M. Saidi, R. H. Abardeh, Air pressure dependence of natural-convection heat transfer, *Proceedings of the World Congress on Engineering* 2010 II.

- [133] G. Scranton, T. P. Xiao, V. Ganapati, J. Holzrichter, P. F. Peterson, E. Yablonovitch, Highly efficient thermophotovoltaics enabled by photon re-use, in: 2016 IEEE 43rd Photovoltaic Specialists Conference (PVSC), 2016, pp. 1026–1029. doi:10.1109/PVSC.2016.7749766.
- [134] G. L. Araujo, A. Marti, Absolute limiting efficiencies for photovoltaic energy conversion, *Sol. Energy Mater Sol. Cells* 33 (1994) 213–240.
- [135] W. Shockley, H. J. Queisser, Detailed balance limit of efficiency of p-n junction solar cells, *J. Appl. Phys* 32 (1961) 510–519.
- [136] J. Wang, B. Wei, Q. Wei, D. Li, Optical property and thermal stability of Mo/Mo-SiO₂/SiO₂ solar-selective coating prepared by magnetron sputtering, *Physica Status Solidi A* 208 (2011) 664–667.
- [137] A. Lenert, D. M. Bierman, Y. Nam, W. R. Chan, I. Celanovic, M. Soljacic, E. N. Wang, A nanophotonic solar thermophotovoltaic device, *Nat. Nanotechnol.* 9 (2014) 126–130.
- [138] A. S. Vlasov, V. P. Khvostikov, O. A. Khvostikova, P. Y. Gazaryan, S. V. Sorokina, V. M. Andreev, TPV systems with solar powered tungsten emitters, *AIP Conference Proceedings* 890 (2007) 327–334.
- [139] H. Yugami, H. Sai, K. Nakamura, H. Nakagawa, H. Ohtsubo, Solar thermophotovoltaic using Al₂O₃/Er₃Al₅O₁₂ eutectic composite selective emitter, *IEEE Photovoltaic Specialists Conference* 28 (2000) 1214–1217.
- [140] A. Datas, C. Algora, Development and experimental evaluation of a complete solar thermophotovoltaic system, *Progress in Photovoltaics: Research and Applications* 890 (2012) 327–334.
- [141] S. Lin, J. Moreno, J. G. Fleming, Three-dimensional photonic-crystal emitter for thermal photovoltaic power generation, *Appl. Phys. Lett.* 83 (2003) 380–382.

- 1295 [142] C. Wu, B. N. III, J. John, A. Milder, B. Zollars, S. Savoy, G. Shvets, Metamaterial-based integrated plasmonic absorber/emitter for solar thermo-photovoltaic systems, J. Optics 14 (2012) 24005–24008.
- [143] C. Ungaro, S. K. Gray, M. C. Gupta, A solar thermophotovoltaic system using nanostructures, Opt. Express 23 (2015) A1149–A1156.